ORNL/TM-2002/215

Final Report: Advanced Ion Trap Mass Spectrometry Program

October 2002

Stephen A. Lammert
Marcus B. Wise
William B. Whitten
James L. Stephenson
Cyril V. Thompson
Scott A. McLuckey
John S. Wagner

ORNL/TM-2002/215

Oak Ridge National Laboratory
Chemical Sciences Division

FINAL REPORT: ADVANCED ION TRAP MASS SPECTROMETRY PROGRAM

Stephen A. Lammert
Marcus B. Wise
William B. Whitten
James L. Stephenson
Cyril V. Thompson
Scott A. McLuckey
John S. Wagner, Sandia National Laboratories

Date Published—October 2002

Prepared for the U.S. Department of Energy,
Office of Nonproliferation Research and Engineering (NA-22),
Chemical and Biological National Security Program

Prepared by
OAK RIDGE NATIONAL LABORATORY
P.O. Box 2008
Oak Ridge, Tennessee 37831-6285
managed by
UT-Battelle, LLC
for the
U.S. DEPARTMENT OF ENERGY
under contract DE-AC05-00OR22725

CONTENTS

LIST OF FIGURES

LIST OF TABLES

ACKNOWLEDGMENTS

Research for the Advanced Ion Trap Mass Spectrometry Program was funded by the U.S. Department of Energy, Office of Nonproliferation Research and Engineering (NA-22), Chemical and Biological National Security Program. The authors would like to thank Wolfgang Plass and Graham Cooks at Purdue University for their help in optimizing the toroid geometry.

EXECUTIVE SUMMARY

This report covers the three main projects that collectively comprised the Advanced Ion Trap Mass Spectrometry Program.

Chapter 1 describes the direct interrogation of individual particles by laser desorption within the ion trap mass spectrometer analyzer. The goals were (1) to develop an "intelligent trigger" capable of distinguishing particles of biological origin from those of nonbiological origin in the background and interferent particles and (2) to explore the capability for individual particle identification.

Summary Direct interrogation of particles by laser ablation and ion trap mass spectrometry was shown to have good promise for discriminating between particles of biological origin and those of nonbiological origin, although detailed protocols and operating conditions were not worked out. A library of more than 20,000 spectra of various types of biological particles has been assembled. Methods based on multivariate analysis and on neural networks were used to discriminate between particles of biological origin and those of nonbiological origin. It was possible to discriminate between at least some species of bacteria if mass spectra of several hundred similar particles were obtained.

Chapter 2 addresses the development of a new ion trap mass analyzer geometry that offers the potential for a significant increase in ion storage capacity for a given set of analyzer operating conditions. This geometry may lead to the development of smaller, lower-power field-portable ion trap mass spectrometers while retaining laboratory-scale analytical performance.

Summary A novel ion trap mass spectrometer based on toroidal ion storage geometry has been developed. The analyzer geometry is based on the edge rotation of a quadrupolar ion trap cross section into the shape of a torus. Initial performance of this device was poor, however, due to the significant contribution of nonlinear fields introduced by the rotation of the symmetric ion-trapping geometry. These nonlinear resonances contributed to poor mass resolution and sensitivity and to erratic ion ejection behavior. To correct for these nonlinear effects, the geometry of the toroid ion trap analyzer has been modified to create an asymmetric torus, as first suggested by computer simulations that predicted significantly improved performance and unit mass resolution for this geometry. A reduced-sized version (one-fifth scale) has been fabricated but was not tested within the scope of this project.

Chapter 3 describes groundbreaking progress toward the use of ion-ion chemistry to control the charge state of ions formed by the electrospray ionization process, which in turn enables precision analysis of whole proteins. In addition, this technique may offer the unique possibility of a priori identification of unknown biological material when employed with existing proteomics and genomic databases.

Summary Ion-ion chemistry within the ion trap was used to reduce the ions in highly charged states to states of +1 and +2 charges. Reduction in charge greatly simplifies identification of molecular weights of fragments from large biological molecules. This technique enables the analysis of whole proteins as biomarkers for the detection and identification of all three classes of biological weapons (bacteria, toxins, and viruses). In addition to methods development, tests were carried out with samples of tap water, local creek water, and soil (local red clay) spiked with melittin (bee venom), cholera toxin, and virus MS2. All three analytes were identified in tap water and soil; however, all three were problematic for detection in creek water at concentrations of 1 nM. More development of methods is needed.

ADVANCED ION TRAP PROGRAM PUBLICATIONS SPONSORED BY THE U.S. DEPARTMENT OF ENERGY CHEMICAL AND BIOLOGICAL NATIONAL SECURITY PROGRAM

Individual Particle Analyzer

Mo Yang, William B. Whitten, and R. W. Shaw, "Real-Time Chemical Analysis of Aerosol Particles," *SPIE Proceedings of Advanced Optical Methods for Ultrasensitive Detection,* Vol. 2385, February 6–7, 1995, San José, Calif., pp. 51–58.

Mo Yang, John M. Dale, William B. Whitten, and J. Michael Ramsey, "Laser Desorption Mass Spectrometry of a Levitated Single Microparticle in a Quadrupole Ion Trap," *Anal. Chem.* 67, 1021 (1995).

Mo Yang, William B. Whitten, and J. Michael Ramsey, "Quadrupole Trap Control Circuit for Laser Desorption Mass Spectrometry of Levitated Microparticles," *Rev. Sci. Instrum.* 66, 5222 (1995).

Mo Yang, John M. Dale, William B. Whitten, and J. M. Ramsey, "Laser Desorption Tandem Mass Spectrometry of Individual Microparticles in an Ion Trap Mass Spectrometer," *Anal. Chem.* 67, 4330 (1995).

Mo Yang, P. T. A. Reilly, K. B. Boraas, W. B. Whitten, and J. M. Ramsey, "Real-Time Chemical Analysis of Aerosol Particles Using an Ion Trap Mass Spectrometer," *Rapid Comm. In Mass Spectrom.* 10, 347 (1996).

Mo Yang, Peter T. A. Reilly, Rainer Gieray, William B. Whitten, and J. Michael Ramsey, "Complete Chemical Analysis of Aerosol Particles in Real-Time," *J Korean Physical Society*, 30/2, 359 (1997).

R. A. Gieray, P. T. A. Reilly, M. Yang, W. B. Whitten, and J. M. Ramsey, "Real-Time Detection of Individual Airborne Bacteria," *J. Microbiol. Methods* 29, 191 (1997).

P. T. A. Reilly, R. A. Gieray, W B. Whitten, and J. M. Ramsey, "Real-Time Characterization of the Organic Composition and Size of Individual Diesel Engine Smoke Particles," *Environ. Sci. Technol.* 32, 2672 (1998).

A. C. Lazar, P. T. A. Reilly, W. B. Whitten, and J. M. Ramsey, "Real-Time Surface Analysis of Individual Airborne Environmental Particles," *Environ. Sci. Technol.* 33, 3993 (1999).E. P. Parker, M. W. Trahan, J. S. Wagner, S. E. Rosenthal, W. B. Whitten, R. A. Gieray, P. T. A. Reilly, A. C. Lazar, and J. M. Ramsey, "Detection and Classification of Individual Airborne Microparticles Using Laser Ablation Mass Spectroscopy and Multivariate Analysis," *Field Analytical Chemistry and Technology,* 4, 31 (2000).

A. C. Lazar, P. T. A. Reilly, W. B. Whitten, and J. M. Ramsey, "Laser Desorption/In Situ Chemical Ionization Aerosol Mass Spectrometry for Monitoring Tributyl Phosphate on the Surface of Environmental Particles," *Anal. Chem.* 72, 2142 (2000).

P. T. Reilly, R. A. Gieray, W. B. Whitten, and J. M. Ramsey, "Direct Observation of the Evolution of the Soot Carbonization Process in an Acetylene Diffusion Flame via Real-Time Aerosol Mass Spectrometry," *Combustion and Flame* 122, 90 (2000).

P. T. A. Reilly, A. C. Lazar, R. A. Gieray, W. B. Whitten, and J. M. Ramsey, "The Elucidation of Charge-Transfer-Induced Matrix Effects in Environmental Aerosols Via Real-Time Aerosol Mass Spectral Analysis of Individual Airborne Particles," *Aerosol Science and Technology* 33, 135 (2000).

A. C. Lazar, P. T. A. Reilly, W. B. Whitten, and J. M. Ramsey, "Laser Desorption/Ionization Coupled to Tandem Mass Spectrometry for Real-Time Monitoring of Paraquat on the Surface of Environmental Particles," *Rapid Comm. In Mass Spectrom.* 14, 1523 (2000).

P. T. A. Reilly, R. A. Gieray, W. B. Whitten, and J. M. Ramsey, "Fullerene Evolution in Flame-Generated Soot," *J. American Chemical Society* 122, 11596 (2000).

Toroid Mass Analyzer

S.A. Lammert, W. L. Plass, C.V. Thompson and M.B. Wise, "Optimization and Performance of a Toroidal Ion Trap Mass Spectrometer," *Int. Journal Mass Spectrom*. 212 (1–3), 25–40 (2002).

Electrospray Ion-Ion

J. L. Stephenson, Jr., and S. A. McLuckey, "Anion Effects on Storage and Resonance Ejection of High Mass-to-Charge Cations in the Quadrupole Ion Trap" *Anal. Chem.* 69, 3760–66 (1997).

S. A. McLuckey, J. L. Stephenson, Jr., and K.G. Asano, "Ion-ion Proton Transfer Kinetics: Implications for Analysis of Ions Derived from Electrospray of Protein Mixtures" *Anal. Chem.* 70, 1198–1202 (1998).

J. L. Stephenson, Jr., and S. A. McLuckey, "Charge Manipulation for Improved Mass Determination of High Mass Species and Mixture Components by Electospray Mass Spectrometry," *J. Mass Spectrom.* 33, 664–72 (1998).

J. L. Stephenson, Jr., and S. A. McLuckey, "Ion-Ion Reactions for Oligopeptide Mixture Analysis: Applications to Mixtures Comprised of 0.5–100 kDa Components," *J. Am. Soc. Mass Spectrom.* 9, 585–96 (1998).

J. L. Stephenson, Jr., and S. A. McLuckey, "Simplification of Product Ion Spectra Derived from Multiply-Charged Parent Ions via Ion\Ion Chemistry," *Anal. Chem.* 70, 3533–44 (1998).

S. A. McLuckey and J. L. Stephenson, Jr., "Ion-Ion Reactions Involving High Mass Multiply-Charged Ions," *Mass Spectrom. Rev*. 17, 369-407 (1998).

J. L. Stephenson, Jr., B. J. Cargile, and S. A. McLuckey, "Ion Trap Collisional Activation of Disulfide Linkage Intact and Reduced Multiply Protonated Polypeptides" *Rapid Comm. Mass Spectrom.* 13, 2040–48 (1999).

J. L. Stephenson, Jr, B. J.; Cargile, and S. A. McLuckey, "Target Protein Analysis of Bacteriophage MS2 Viral Coat Protein from *E. Coli* Lysates" *Anal. Chem*. 73, 1277–85 (2001).

S. A. McLuckey, J. M. Wells, J. L. Stephenson, Jr., and D. E. Goeringer, "Novel Quadrupole Ion Trap Methods for Characterizing the Chemistry of Gaseous Macro-Ions" *Int. J. Mass Spectrom*. 200, 137–161 (2000).

1. INDIVIDUAL PARTICLE ANALYZER

The airborne particle mass spectrometer is an instrument that performs gas-phase analysis of individual airborne particles on a real-time basis (Yang et al. 1996). The spectrometer uses laser ablation together with ion trap mass spectrometry to analyze individual airborne particles as they enter the instrument. It operates on demand (i.e., each incoming particle triggers the laser ablation and mass analysis process). In principle it should be able to discriminate between bacterial and nonbacterial particles one by one as they enter the apparatus. Thus the instrument could be used as a stand-alone monitor to detect changes in the particulate background or as an operator-directed survey instrument to detect the presence or absence of airborne bacteria. A major role would be as a trigger to initiate a slow but comprehensive analysis of a collected sample to identify a potential threat.

The instrument is expected to be similar in size to a suitcase and to weigh upwards of 100 lb, and thus be transportable. It could be operated with battery or wall power and could be wheeled into a building for surveys in an emergency situation. A slightly different version of the instrument could be installed permanently as a smart sensor in critical locations and networked to a central facility for programming and real-time area monitoring.

A laboratory version of the airborne particle mass spectrometer has been used to acquire single-particle mass spectra of a wide range of samples to aid in the development of discrimination and identification methodology (Gieray et al. 1997). The present spectral library contains more than 20,000 spectra of positive and negative ions from six species of bacteria, one type of bacterial spore, six species of pollen, six standard reference particulate samples from the National Institute of Standards and Technology (NIST), and samples of two other simulants of biological threats used in the field trials at Dugway Proving Ground. The particle types and numbers of data files generated are summarized in Table 1.1.

Table 1.1. Mass spectral library for numerical pattern recognition

Species or particle type	Number of ion spectra	
	Positive	**Negative**
Azotobacter vinlandii	348	686
Bacillus subtilis	853	1107
Escherichia coli	574	518
Enterobacter aerogenes	301	234
Micrococcus lysodeikticus	369	378
Bacillus subtilis (b.g.) spores	689	647
Ambrosia trifida	392	373
Artemisia tridentata	179	154
Betulia alba	178	173
Dactylis glomerata	175	168
Juglans nigra	183	201
Agrostis alba	129	136
NIST 1645	1047	604
NIST 4350b	797	638
NIST 8407	958	632
NIST Montana soil	1049	860
NIST Peruvian soil	693	475
NIST 1648 urban particles	571	516
Pantoea agglomerans	931	715
MS2	987	944

Experiments with aerosolized bacteria show some promise for rapid discrimination of bacteria from particles of nonbiological origin and even perhaps for species identification, as shown in Fig. 1.1. We have teamed with John S. Wagner's group at Sandia National Laboratories to explore the use of intelligent computer algorithms for the detection and/or identification of individual bacteria from the mass spectral data generated by this apparatus. Two numerical techniques for processing the mass spectral data, multivariate patch analysis (MPA) and genetically trained neural networks, are being evaluated.

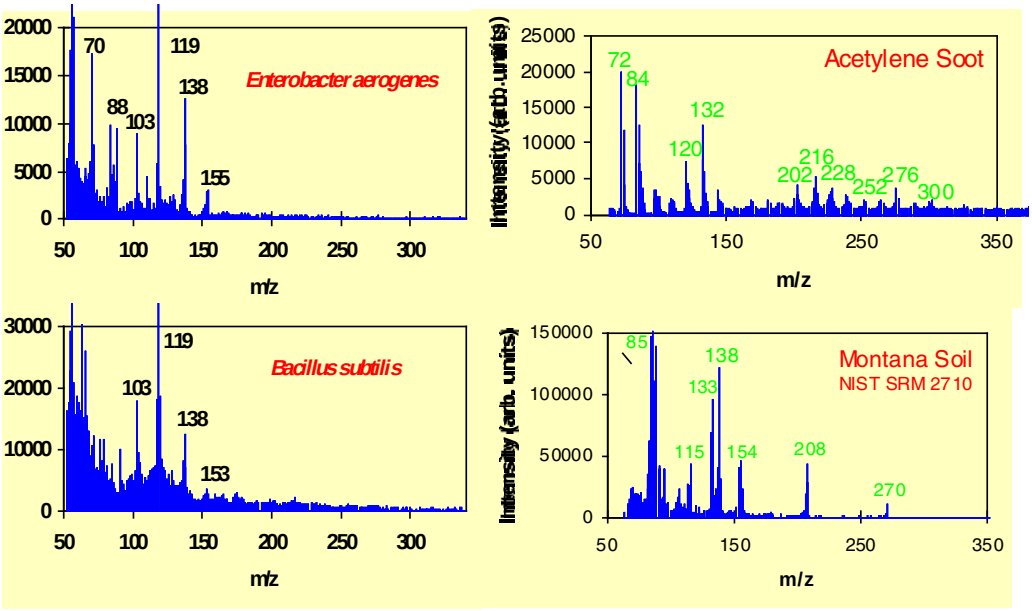

Fig. 1.1. The mass spectra of different species of bacteria are similar to each other but quite different from mass spectra of nonbacterial particles.

MPA is a variant of traditional multivariate analysis in which certain spectral regions or "patches" can be selected for optimum selectivity (Parker et al. 2000). The patch selection is performed by a genetic algorithm operating on training sets of spectra. For the results presented here, the complete spectra were used. To test the method, half of the spectra from a given run for one type of particle and ion polarity were averaged to obtain reference mass spectra. The other half were averaged to generate trial spectra. MPA was used to find the "concentration" of each of the reference spectra in a given trial spectrum (ideally unity for the corresponding particle type and zero for all others). This process was repeated for different sets of runs and for cases where the reference and trial spectra came from different runs. We also used spectra combining ions of both polarities to simulate results that would be obtained if spectra of both polarities could be measured on the same particle.

MPA results for a set of spectra generated from one run for each particle type are shown in Table 1.2 (Parker et al. 2000). For this set of spectra, all of the particles were correctly identified and spectra with combined ion polarities gave higher scores than either polarity alone. For 3 runs out of 36 where the reference and trial spectra came from separate data sets, the particles were incorrectly identified, at least two due to recognizable instrumental problems that arose during a run. All particles were correctly identified with the combined spectra in spite of the bad runs, but the scores were not as high as for the set shown in Table 1.2.

The second approach we have taken for particle classification or identification is by the use of a feed-forward neural network. Neural networks can be assembled and trained to give a binary output in which the input data are separated into two classes. In this mode, the success of the airborne particle mass spectrometer as a bacterial counter depends on its ability to make a classification decision for each

Table 1.2. Multivariate patch analysis scores for positive-ion, negative-ion, and combined-mass spectra[a]

Species or particle type	Positive ions	Negative ions	Combined spectra
Azotobacter vinlandii	A	A	A
Bacillus subtilis	C	B	A
Escherichia coli	A	A	A
Enterobacter aerogenes	A	C	A
Micrococcus lysodeikticus	A	C	A
Bacillus subtilis (b.g.) spores	A	B	A
Ambrosia trifida	A	A	A
Artemisia tridentata	A	B	A
Betulia alba	A	C	A
Dactylis glomerata	A	A	A
Juglans nigra	A	B	A
Agrostis alba	A	A	A
NIST 1645	B	A	A
NIST 4350b	A	C	A
NIST 8407	A	B	A
NIST Montana soil	A	C	A
NIST Peruvian soil	B	A	A
NIST 1648 urban particles	B	C	B

[a]The grades have the following meanings.

A: the calculated concentration of the correct particle type was approximately 1.0 and all other particles were below 0.15.

B: all particles other than the correct type gave concentrations below 0.33 of the maximum concentration.

C: the correct type gave the largest concentration but one or more of the other particles had concentrations greater than 0.33 of the maximum concentration.

particle. Although further identification of each particle is obviously desirable, the similarity of mass spectra from different species of bacteria and the shot-to-shot variations make this difficult. We are hopeful that the apparent similarity of bacterial mass spectra obtained in our real-time laser ablation mass spectrometer will enable their recognition as a class even if further identification is not possible.

In our neural network experiments with averaged spectra, the six bacterial species could be successfully discriminated from all of the other types of particles. The training sets were 75 particle averages of one bacterial species, one pollen species, and two NIST standards. The neural network had 66 input neurodes and 67 hidden-layer neurodes, giving a mass resolution of 5 Da.

In later tests, a neural network trained with averaged spectra was then challenged with single-particle mass spectra from the library (e.g, Fig. 1.2). Seventy-five spectra were selected and averaged for each of 18 types of particles in our library. The neural network was trained with the 18 averaged spectra. Preliminary results were obtained by challenging the network with single-particle spectra. This preliminary experiment yielded some errors on individual particles; however, we found that false alarms can be reduced substantially by combining the results for several particles. This experiment also demonstrated that it is possible to adjust the ratio of false positives to false negatives to fit the conditions of deployment. In principle, our apparatus can now make an unassisted real-time classification decision (although not yet always correct) on each incoming aerosol particle that is analyzed as to whether or not it is a bacterium.

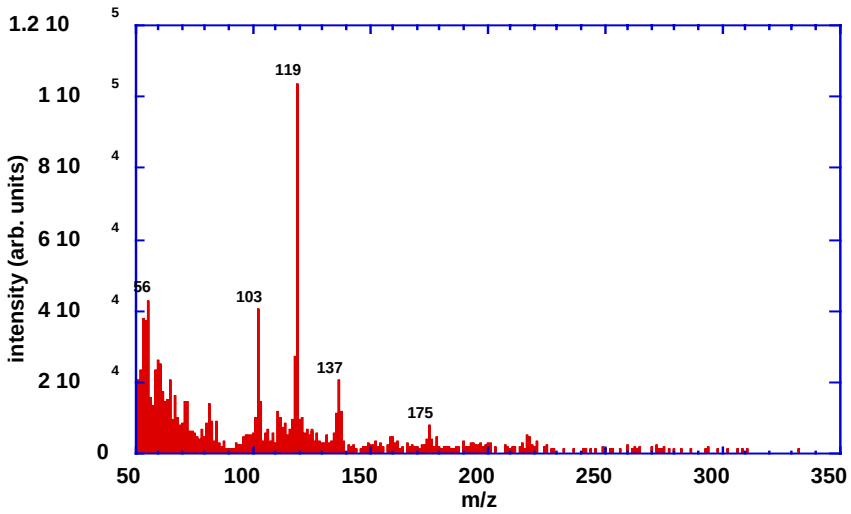

Fig. 1.2. Mass spectrum of a single *B. subtilis* cell.

For a test of our ability to distinguish bacterial from nonbacterial particles in a real sample, we analyzed some samples collected from occupational environments in collaboration with Dr. B. T. Chen and coworkers, Health Effects Laboratory Division, at the National Institute for Occupational Safety and Health. The three principal classes of particles studied were dust collected from a poultry house, cotton dust, and aerosols of metalworking fluids. The primary objective was to see if microorganisms could be detected in single-particle measurements on these real samples. The samples were introduced into the airborne-particle mass spectrometer both as dry aspirated powder and as a dried aerosol from a nebulized aqueous suspension. Little difference was found between the two methods of introduction.

An average of 220 mass spectra of the poultry house dust is shown in Fig. 1.3. There is almost a continuous distribution of ion masses, thereby making analysis of the total sample tenuous. However, when the spectra are looked at individually, several patterns become apparent. For example, the spectrum shown in Fig. 1.4 is the average of the mass spectra of 31 particles that resembled bacterial mass spectra. The similarity of this spectrum with that of a single *Bacillus subtilis* spectrum (Fig. 1.2) is noteworthy, although some differences suggest the presence of different species. Negative-ion spectra show a class of particles with a high concentration of a species giving a peak at m/z –169 that we attribute to uric acid, a common constituent of guano. There is a strong unidentified peak at m/z 83 in some of the particles.

Considerably more analytical information could have been obtained during the particle mass spectrometry. For example, to identify the peak at m/z –83 in the poultry house dust, that particular ion could have been collisionally dissociated and the fragment ion spectrum determined to assist in the identification. The diversity of the single-particle spectra for the mixed-particle samples emphasizes the need for machine algorithms for on-line particle classification.

In summary, we have shown that the laboratory-based airborne particle mass spectrometer can measure the size and mass spectrum of individual airborne particles in real time for samples that are brought to the instrument. The true potential of the method will only be manifest, however, when a transportable version that can be operated in situ has been completed. The measurements are triggered by the particle's entry into the instrument, and the system can operate unattended as a continuous monitor. It can also be operated as a manual survey instrument. An operator can change the instrument's operating conditions so

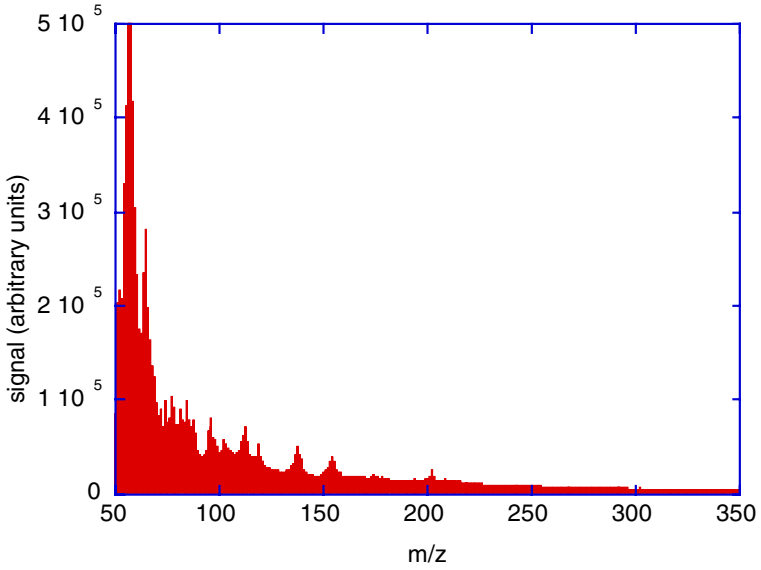

Fig. 1.3. Averaged mass spectrum of 220 poultry house dust particles.

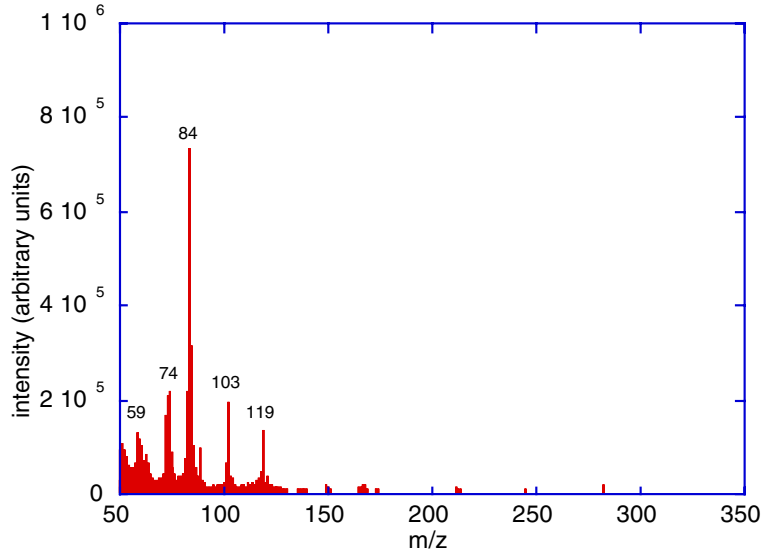

Fig. 1.4. Averaged mass spectrum of 31 particles of poultry house dust that appeared to be bacteria.

that mass spectrometry/mass spectrometry (MS/MS) spectra can be acquired if an interesting series of particles is encountered or if a new target species is selected. We have also shown that computer algorithms can be developed to make a real-time decision as to whether a particle is a bacterium or not based on its mass spectrum.

2. TOROID ION TRAP MASS ANALYZER

Small instrument size, simple ion optics, ultrahigh sensitivity, and the selectivity of MS/MS are just a few of the reasons that ion trap mass spectrometry devices have gained popularity for use as fieldable mass spectrometers. Although laboratory-based ion traps are small compared with other forms of mass spectrometers, efforts to further reduce size, weight, and power are limited to some extent by the tuned radio-frequency (rf) coil that provides the primary rf trapping field. For a given m/z ion, stable trapping ($q \leq 0.91$) requires an rf amplitude that increases as the square of the trapping field radius.

$$q = \frac{-8eV}{m\left(r_0^2 + 2z_0^2\right)\Omega^2} \tag{1}$$

Unfortunately, smaller ion trap analyzers are significantly more prone to degradation of space charge performance arising from ion-ion repulsion. Ion-ion interactions (space charge) limit the performance of ion trap mass spectrometers under conditions of high ion currents. This problem is manifested in many areas of ion trap operation but most commonly at a maximum dynamic range of approximately 10^4. Attempts to mitigate space charge effects have included coincident trapping of both positive and negative ions, but this approach typically requires multiple ion sources. Efforts to make the trapping field larger (increased radius, r_0) to accommodate an increased number of ions are limited by the fundamental equations [(see Eq. (1)] where the ring rf voltage (V) is proportional to the square of the ring radius (r_0). Current rf power supplies are already near the plasma-discharge limit at voltages approaching 15,000 $V_{p–p}$. These same fundamental limitations affect attempts to develop smaller ion trap devices that would operate on considerably less rf power because onset of space-charged conditions would occur at much lower ion concentrations in these smaller devices.

A new ion trap analyzer geometry has been developed (see Fig. 2.1) that is based on the edge rotation of the quadrupole ion trap cross section about the axis indicated by the dashed double-headed arrow in Fig. 2.1 rather than a center rotation about the axis indicated by the solid double-headed arrow. The resulting trapping field is therefore in the shape of a torus. For a given cross-section analyzer radius, the toroid trap will have a significantly greater ion storage region than that in a device with a conventional ion trap geometry. In addition to increased ion storage capacity, this geometry has a new degree of freedom in ion motion (within the dimension of the toroid) that may offer new opportunities in ion-injection and ion-activation experiments. Finally, the toroidal ion trap design may allow the reduction of the trapping field radius (with a corresponding reduction in rf power) while maintaining a large ion-storage capacity. This toroidal geometry is in contrast to a similar device based on the cyclization of a linear quadrupole.

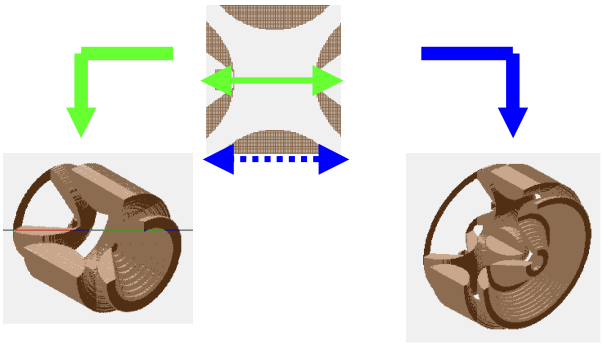

Fig. 2.1. Diagram showing evolution of toroidal ion trap geometry.

2.1 Symmetric Toroid

A prototype version of the toroid analyzer was constructed with a geometry based on a standard ion trap cross section with a 1-cm radius, which is the same as most commercial ion trap systems (see Figs. 2.2 and 2.3). The toroid ion trap used a standard electronic system (ITMS™, Finnigan-MAT, San José,

Fig. 2.2. Photograph of prototype toroidal ion trap.

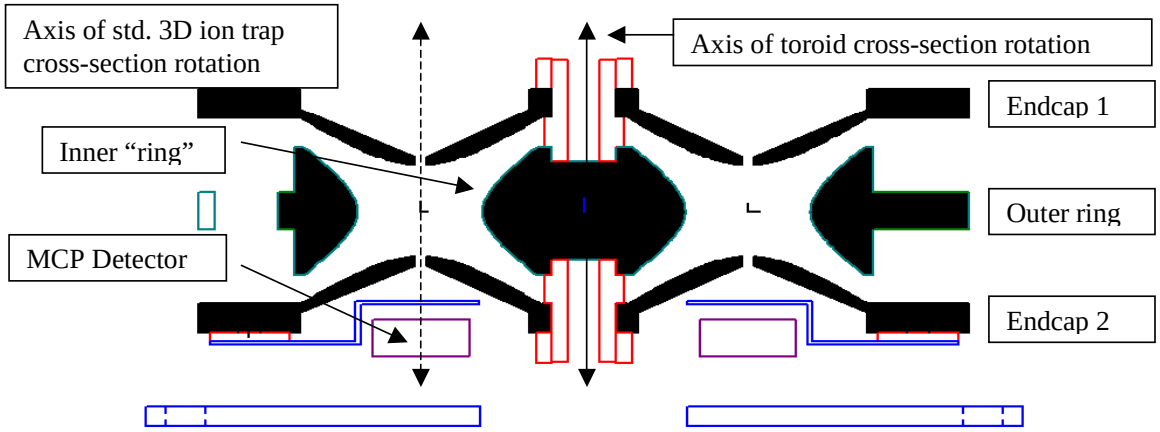

Fig. 2.3. Cross-sectional drawing of prototype toroidal ion trap.

Calif.) with a custom vacuum chamber. Because the r_0 of the device is 1 cm (same as the standard Finnigan ITMS), only minimal changes are required to the operating electronics of the instrument. However, the capacitance of the toroid ion trap analyzer increased from about 25 pf to 34 pf, and thus the rf control circuitry required modifications, which included retapping of the rf drive coil and modification of the rf drive frequency from 1.1 MHz to 976 KHz. Frequency modification was accomplished by using a Hewlett-Packard model 3325 Frequency Synthesizer/Function Generator (Hewlett-Packard, Palo Alto, Calif.). The ion source and detection circuitry required no modification. The ITMS filament assembly was fitted directly above the slit on the upper endcap with only mounting modifications. Because the ions exit through an annular slit, a custom multichannel plate detector was fabricated and was used to detect the ejected ions.

The mass analysis performance of this analyzer was characterized by broad mass peaks, the intensity and resolution of which were strongly dependent on the supplemental ac ejection parameters (β_{eject}-values). In this version, no attempt was made to correct for field imperfections that would be introduced from the rotation of the ion-trapping field. The mass analysis performance of the symmetric toroid ion trap delivers a mass resolution ofabout 1 to 2 amu FWHM, as is shown in the spectrum for benzene given in Fig. 2.4.

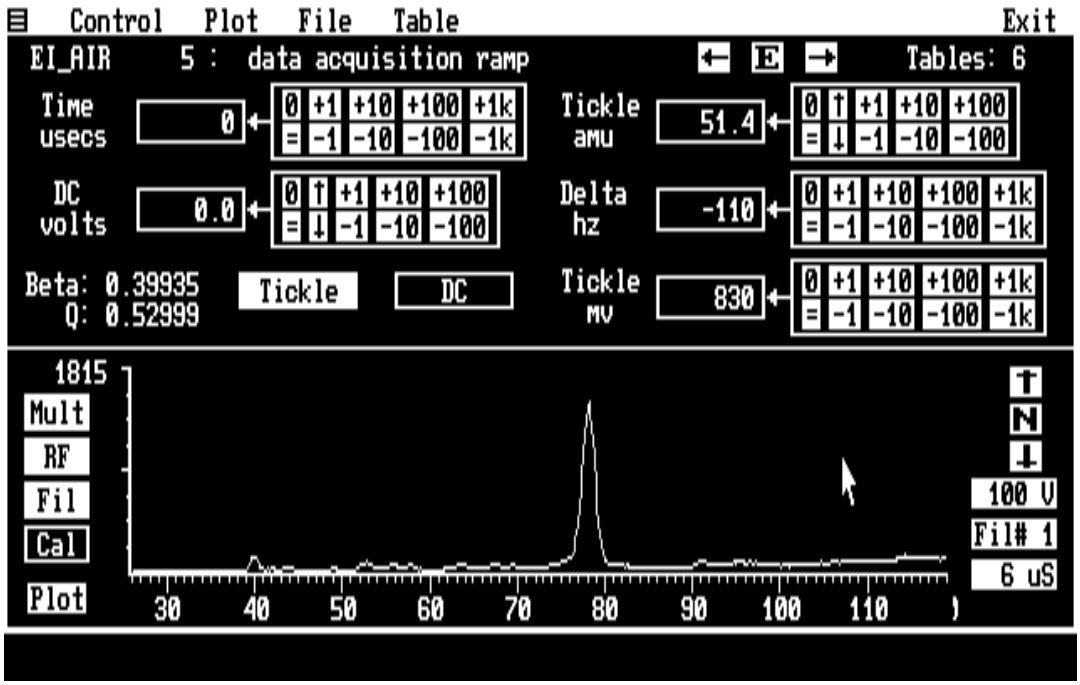

Fig. 2.4. Mass spectrum of benzene obtained with symmetrical toroidal ion trap.

The mass resolution is further demonstrated in the spectrum in Fig. 2.5 for n-butyl benzene, which shows two intense ions at m/z 91 and 92. As can be seen, the ions at m/z 91 and 92 are unresolved in this spectrum. The spectrum is compared with a reference spectrum from the Wiley Mass Spectrometry Database.

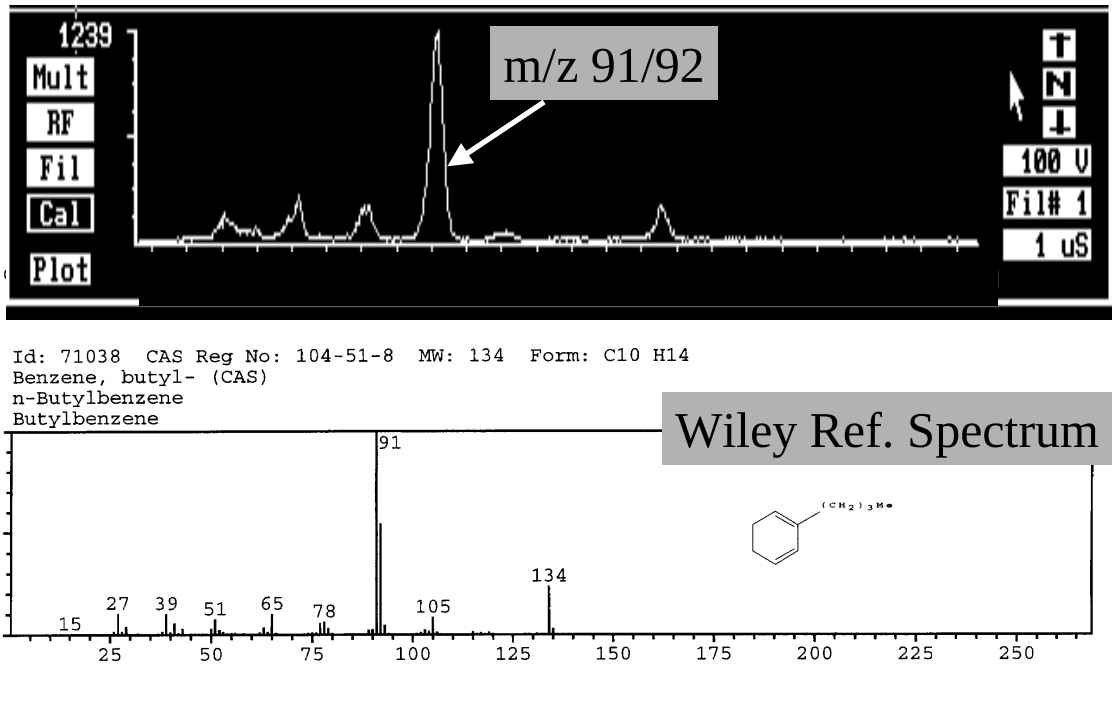

Fig. 2.5. Mass spectrum of n-butyl benzene obtained with symmetrical toroidal trap.

In addition to the poor mass resolution, the spectrum is extremely sensitive to the operating pressure and β_{eject}-values. The optima are 3×10^{-6} torr and 0.39, respectively. At discrete β_{eject}-values, severe peak splitting occurred (see Fig. 2.6). At some β_{eject}-values, the mass peaks disappeared altogether.

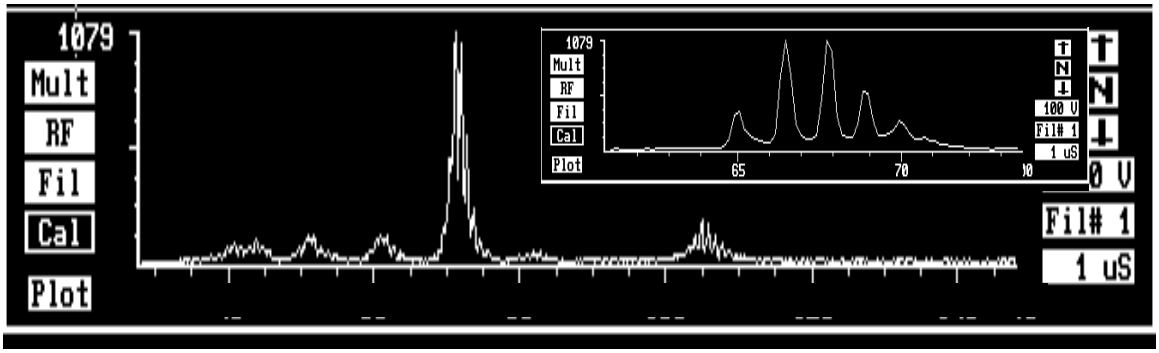

Fig. 2.6. Example of peak splitting.

2.2 Trapping Field Simulation and Optimization

Several possible sources of the poor mass resolution and observed peak splitting have been considered. These include

- nonlinear fields resulting from the curved quadrupolar field geometry,
- nonsymmetrical trapping field,
- alignment errors (nonparallel components),
- electrode machining imperfections (the device may require tolerances similar to those in linear quadrupoles), and
- multiple (four) discrete trapping volumes from the four separate slits on the filament and detector endcap created by the "bridges."

SIMION 3D6 was used to simulate the device's ability to trap ions formed from a point source [see Fig. 2.7 (a)], allowing time for diffusion (b), and then kinetically cooling them to the center of the device (c).

In each case, the ion population settles to the bottom of the potential well at a radial position that is inside (closer to the inner ring electrode) the physical center of the trap (the crosshair position in Fig. 2.8) by 10% of the r_0 dimension. In the axial dimension, the ions settle to a point that is in the exact axial center of the device, as seen in Fig. 2.9.

Although the SIMION ion optics program was able to shed light on the location of the potential minimum within the toroid ion trap, it had insufficient analytical capabilities to describe the general trapping field characteristics. Commercial ion traps have a trapping field with a nearly linear growth in the field strength as a function of position (i.e., distance from center of the trapping field). It can be described as an essentially quadrupolar trapping field. It was discovered early in ion trap development that the superposition of a small, positive nonlinear (mostly octapole) field improved the performance of the device. Traditionally, this improvement has been accomplished by intentionally distorting (stretching) either the endcap distance or electrode asymptote angles.

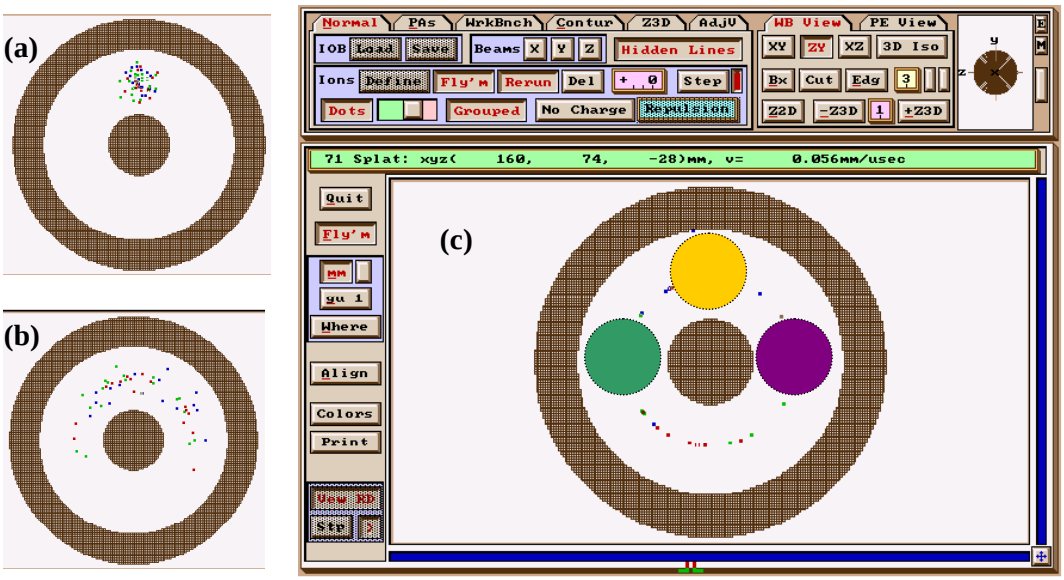

Fig. 2.7 SIMION 3D6 calculation of ion distributions at different times.

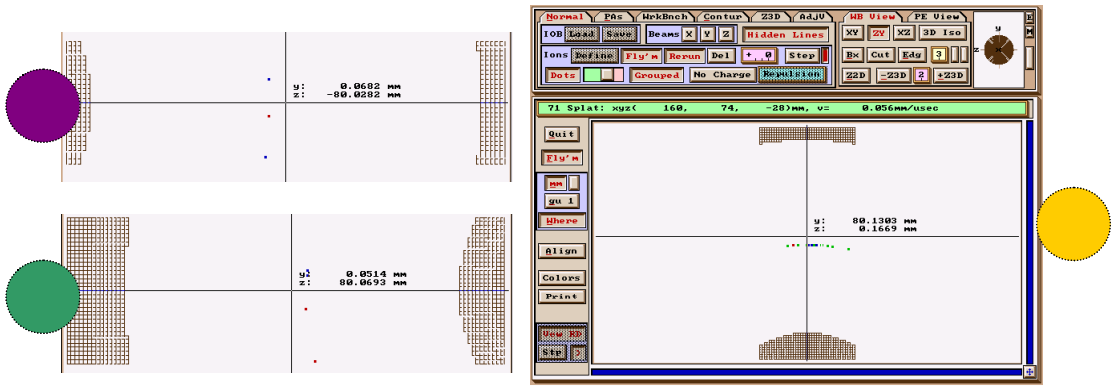

Fig. 2.8. SIMION simulation of ion distribution in radial dimension.

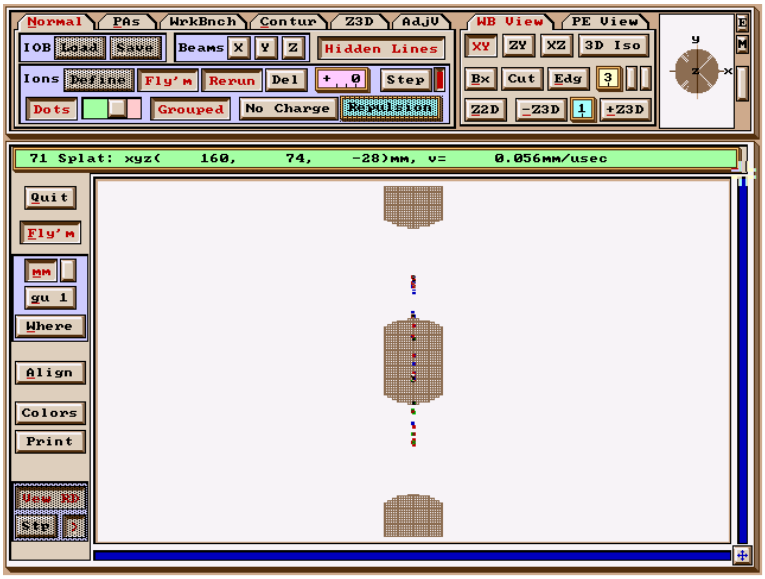

Fig. 2.9. SIMION simulation of ion distribution in the axial dimension.

In collaboration with Wolfgang Plass and Graham Cooks at Purdue University, we used POISSON (a trapping field analysis program developed at Los Alamos National Laboratory) and ITSIM (an ion trap trajectory simulation program developed at Purdue University) to optimize the toroid geometry. These programs revealed that the trapping field in the original, symmetric toroid analyzer had a significant, negative nonlinear component. Using the POISSON field analysis programs, we corrected the field faults by intentionally skewing the cross-sectional symmetry of the device. In this case, the angle of the asymptotes that correspond to the outer ring electrode was decreased while the angle of the asymptotes corresponding to the inner ring electrode was increased until a slight, positive nonlinear field was achieved. This is shown in in Fig. 2.10, in the comparison of the analyzer cross sections of the original symmetrical ion trap (left) with the optimized, asymmetric ion trap (right). Furthermore, ion trajectory simulations using ITSIM indicated that the mass resolution and sensitivity of this asymmetric analyzer would be dramatically improved.

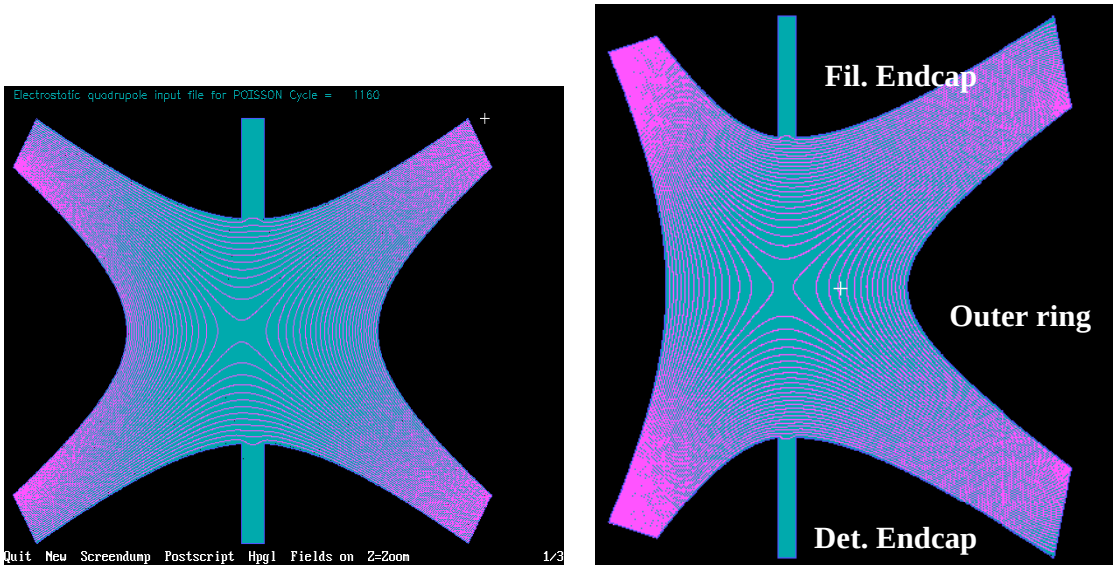

Fig. 2.10. Cross sections of symmetrical and distorted toroidal ion traps.

Based on the simulated optimized parameters, we fabricated an asymmetric version of the toroid ion trap analyzer. A schematic of the assembled analyzer is shown in Fig. 2.11. Indeed, improved performance has been realized by using the newly constructed asymmetric toroidal ion trap analyzer. Figure 2.12 shows the spectrum for n-butylbenzene with strong signal intensity and unit resolution (see inset) at a sample pressure of 9×10^{-7} torr and an ionization time of 25 ms. The spectrum is directly comparable with the spectrum in Fig. 2.5, which was obtained on n-butylbenzene on the original symmetrical ion trap. A full discussion on the theory used to develop the optimization approach, the software used for optimization, and the results obtained has been published in the *International Journal of Mass Spectrometry* (Lammert 2001).

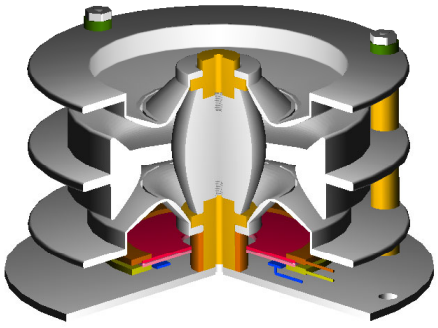

Fig. 2.11. Drawing of improved toroidal ion trap.

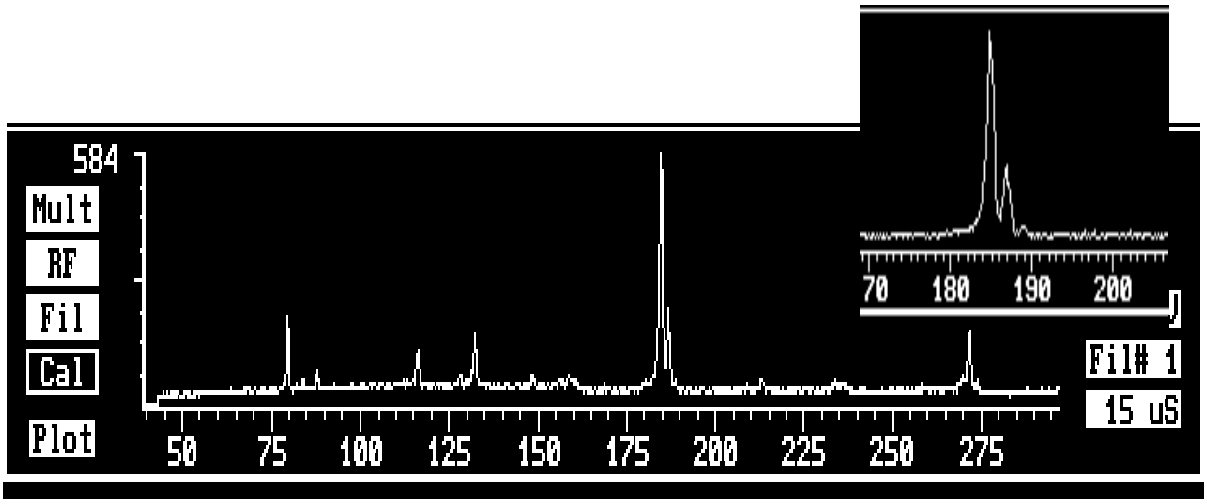

Fig. 2.12. Mass spectrum of n-butylbenzene obtained with the improved toroidal ion trap. (Mass scale given in arbitrary units.)

2.3 Status and Prospects

The improved mass resolution and performance results obtained on the asymmetric version of the ion trap offer promise for a reduced-sized version that would operate on significantly lower voltage while retaining ion-storage capacities comparable to or exceeding those of current commercial ion trap mass spectrometers. In addition, new modes of ion activation may be possible with this design that could have a substantial impact on ion kinetic energies (and thus internal energy deposition) in MS/MS technology.

3. THE USE OF ION-ION CHEMISTRY IN AN ELECTROSPRAY ION TRAP MASS SPECTROMETER FOR THE DETECTION AND IDENTIFICATION OF BIOLOGICAL THREATS

3.1 Ion-Ion Chemistry

The advantages of using a custom-built electrospray ion trap mass spectrometer for the analysis of toxins, viruses, bacteria, and other agents related to biological warfare are discussed. The enabling feature of this instrument is the use of ion-ion reactions within the ion trap to reduce the complexity of overlapping charge states resulting from the electrospray analysis of complex mixtures. The use of ion-ion chemistry allows the reduction or elimination of many time-consuming sample-processing and separation steps often required for analysis by electrospray mass spectrometry.

3.1.1 Introduction

Mass spectrometry has been employed by the U.S. Army as a detector for chemical and biological warfare agents for many years now. Recently, the U.S. Army Soldier Biological and Chemical Command (SBCCOM) funded the development of a second-generation ion trap mass spectrometer called the Block II Chemical and Biological Mass Spectrometer (or Block II CBMS) at Oak Ridge National Laboratory (Hart et al. 2000). This fieldable and ruggedized mass spectrometer uses pyrolysis coupled with a chemical-ionization ion trap mass spectrometer to analyze thermally liberated biomarkers. Although this method works well for bacteria, the analysis of toxins and viruses is more problematic. In another program, discussed here, we have begun to investigate the advantages of using electrospray ionization and ion trap mass spectrometry for the analysis of these materials.

To fully understand the advantages of the electrospray ion trap approach, the limitations of the U.S. Army's Block II CBMS must be understood. The Block II CBMS uses pyrolysis (thermolysis) to liberate the various biomarkers from the targeted agents (Barshick et al. 1999). These biomarkers must be compatible with the gas phase because they are transmitted through heated transfer lines to the mass spectrometer. The primary biomarkers for bacteria are the fatty acids that compose the cell wall. The analysis of fatty acids (after derivatization using a methylating agent to convert the fatty acids to their methyl esters) for identification of bacteria is well established in the fatty acid methyl ester (FAME) analysis technique (Basile et al. 1998). This method for bacteria analysis is easily translated to mass spectrometry because the methyl esters of fatty acids can be easily volatilized. However, the identification of protein toxins and viruses cannot be achieved through the analysis of low-molecular-weight biomarkers that are easily transported through the heated sample path. Currently with the Block II CBMS, protein toxins must be analyzed by determining the relative proportions of two-amino-acid diketopiperazines that are formed in the gas phase by decomposition of the protein. Thus the unique primary sequence information of the protein is lost during this thermal degradation. The problem is the same when analyzing viruses, which are composed primarily of proteins and RNA or DNA. Because the Block II CBMS uses relative intensities of these fragment ions, the method is especially prone to performance degradation in complex environments or if mixtures of proteins are to be analyzed.

In contrast, the electrospray/ion trap mass spectrometry approach targets proteins from all three classes of biological weapons as biomarkers for the presence of a specific organism or toxin (Stephenson et al. 1999, Cargile et al. 2000). It is based on the hypothesis that proteins (either singular or in combination) will be unique to the organism and thus will provide unambiguous identification.

Mass spectrometry can identify proteins by employing a combination of molecular-weight determination and partial protein sequencing. Electrospray mass spectrometry (using an ion trap mass spectrometer) can

provide both molecular weight and partial sequence information in the same analytical method. Electrospray is designed to admit aqueous samples and thus is an appropriate final step after on-line sample preparation techniques, most of which are best performed in the liquid phase. However, electrospray is characterized by the production of a distribution of molecular ions with differing charge states, and thus it can often be difficult to determine the charge state (and thus the molecular weight) of the target species, especially in the presence of complex backgrounds.

The novel enabling technology under development in this program is the use of ion-ion reactions inside the quadrupole ion trap mass analyzer to reduce these multiply charged ions to primarily singly charged ions. In this manner, the complexity of the electrospray spectrum is reduced and the measurement of the molecular weight of the analytes becomes relatively straightforward. Partial sequence information is obtained by performing MS/MS on the individual multiply charged ions, which are especially prone to decomposition due to Coulombic destabilization. The differences in mass of the resulting fragment ions correspond to sequence amino acids from a given protein. By searching databases (either locally developed specific target libraries or the larger web-based databases), identification of the protein is possible if both the molecular weight and the partial protein sequence are used to find a match or matches in the database. In this respect, this method offers the unique possibility of a priori identification of unknown proteins from unknown organisms.

3.1.2 Experimental Methods

Minimal sample preparation and preseparation are desired outcomes of using the ion-ion electrospray ion trap approach. Currently, as performed in the laboratory, the sample-processing steps (and approximate times in parenthesis) can be categorized as follows:

1. buffering/preparation (1 min),
2. lysing (< 10 min),
3. reduction/denaturization (1 min), and
4. final cleanup (1–2 min).

The buffering/preparation step currently consists of adding to the sample to be analyzed (1) tris as a buffer, (2) dithiothreitol to reduce the disulfide bonds, and (3) guanidine HCl to denature the protein and allow dissolution. Currently, the lysing step is performed using a “bead beating” technique, but a “French press” step at 10 kpsi may be an alternative to lysozyme for rapid lysing of bacteria. Next, the solution is heated to 90°C for 1 min. A centrifugation step is currently employed remove cellular debris followed by a quick partition of the sample by employing either a “zip-tip” pipette or dialysis. The broad applicability of both techniques is under study. At that point, the sample is available for electrospray ion trap MS analysis. The final volume of sample is typically about 10 μL. This amount of sample is sufficient for several hours of nanospray electrospray ion trap investigation (athough this amount of time is not required).

3.1.3 Electrospray Ion Trap MS Instrument

The electrospray ion trap mass spectrometer has been custom-built at ORNL and consists of a nanospray syringe pump, the electrospray source (high-voltage needle, skimmers, differentially pumped vacuum), an ion-introduction lens system for ion desolvation and ion focusing, and the custom ion trap mass spectrometer based on a modified Finnigan ITMS. A second, supplemental negative ion introduction source (a small glow-discharge source with perfluoro-1,3-dimethylcyclohexane, PDCH) administers negative ions through an aperture in the ring electrode. A schematic of this system is shown in Fig. 3.1.

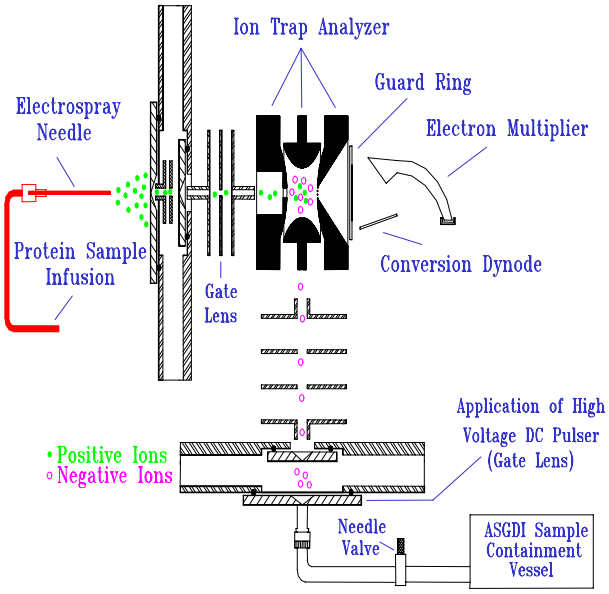

Fig. 3.1. Schematic of the electrospray ion trap mass spectrometer modified with an atmospheric sampling glow discharge negative ionization source.

3.1.4 Results

3.1.4.1 Tobacco Mosaic Virus

The utility of this approach is demonstrated in Fig. 3.2. The electrospray mass spectrum of the coat protein from tobacco mosaic virus is shown in the upper portion of the figure. It contains charge states from +8 to +13. The lower portion of the figure shows the result after the ion-ion reaction. The charge distribution has shifted to primarily the +1 and +2 charge states. The molecular weight of the coat protein of the tobacco mosaic virus can be easily determined from the +1 charge state, and the charge state determination is unambiguous.

3.1.4.2 MS2 in *E. coli*

Bacteriophage MS2 cultures were grown in accordance with standard microbiological techniques. Samples were prepared by passing the MS2-infected media through a 100-kDa spin column and washing the resulting 1-mL fraction with several milliliters of deionized water. DNA/RNA was precipitated with 66% acetic acid, and the resulting complex mixture of viral coat proteins and *E. coli* proteins was analyzed directly. The electrospray mass spectrum both with and without the ion-ion charge reduction step is shown in Fig. 3.3 for the bacteriophage, MS2 in *E. coli*. As shown in the figure, the charge state is reduced from primarily +9 in the conventional electrospray mass spectrum to lower charge states after the ion-ion reaction step.

By performing multiple isolation experiments in conjunction with ion-ion chemistry, a sufficient number of unwanted ions with the same m/z value of the charge state of interest can be removed prior to the

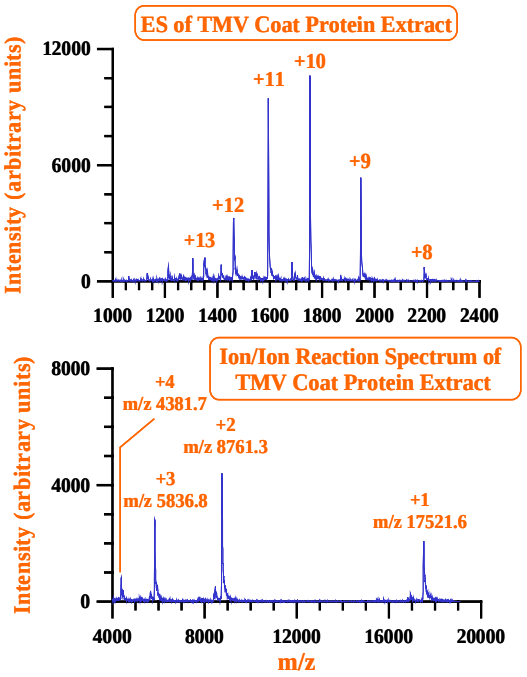

Fig. 3.2. ESI/MS spectrum of the coat protein from tobacco mosaic virus. Top: the normal electrospray spectrum. Bottom: the spectrum after ion-ion charge reduction.

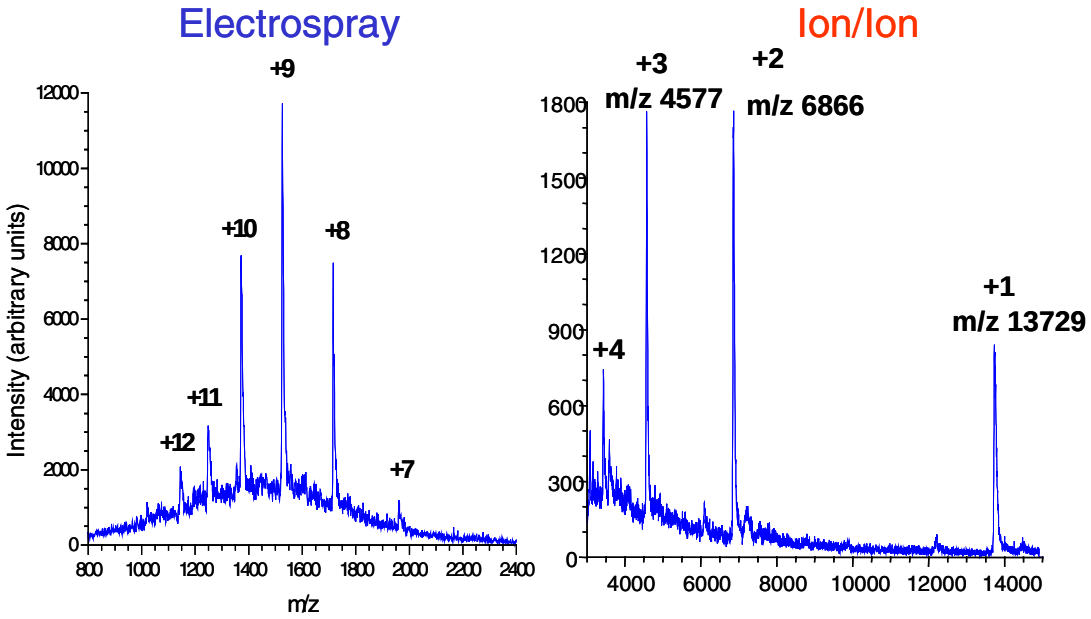

Fig. 3.3. Conventional electrospray mass spectrum (left) and electrospray mass spectrum after ion-ion charge reduction (right) for the analysis of the bacteriophage MS2 in *E. coli.*

MS/MS step. This provides the signal-to-noise ratios necessary for obtaining sequence tag information required to search protein databases. The combination of several MS/MS analyses on a variety of charge states followed by ion-ion reactions can yield unique, charge-state-specific fragmentation to help identify a given protein in the database with an increased confidence level.

The most directly informative structural information is obtained from those charge states that produce a series of product ions arising from fragmentation at adjacent residues. The formation of these product ions via cleavages at adjacent residues is highly dependent upon parent ion charge state. Ion-ion reaction results derived from the collision-induced dissociation of the +8 charge state of the viral MS2 coat protein are shown in Fig. 3.4. Two types of data can be derived from this spectrum. The first is the sequence tag data shown in the inset. This type of data is useful in identifying proteins regardless of whether post-translational modifications are present. It is also useful in checking for genetically modified proteins that may have been engineered in an attempt to evade traditional detection technologies. The second piece of data obtained from this experiment is the presence of the larger fragment ions labeled as y_{37}, b_{92}, b_{116}, and b_{118} (see arrows in Fig. 3.4).

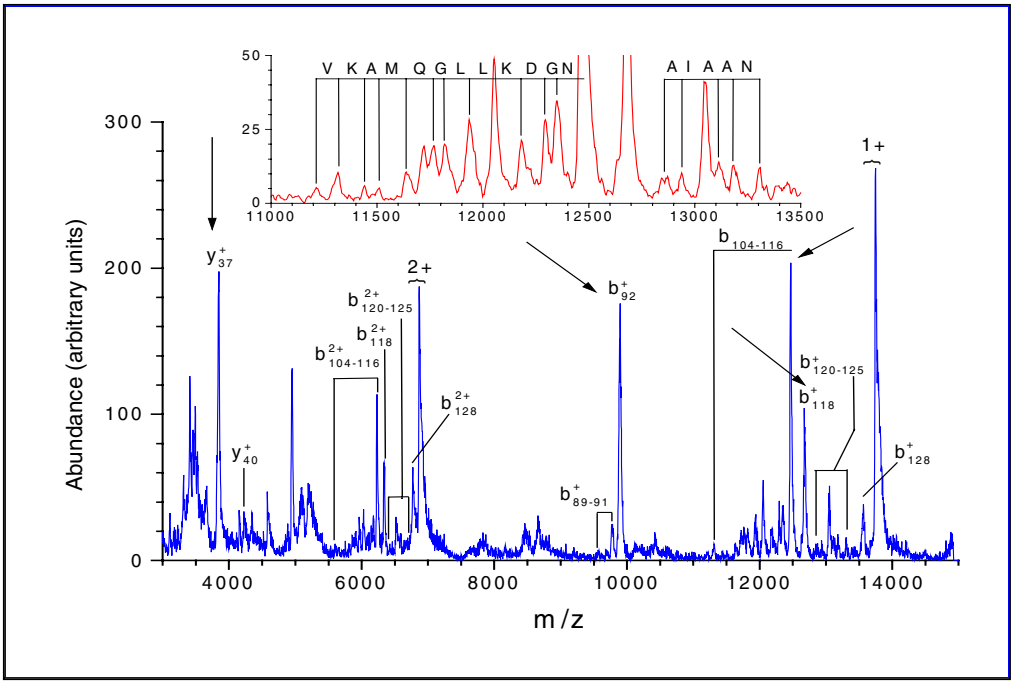

Fig. 3.4. MS/MS of the +8 charge state of the viral coat protein of MS2 showing primary fragments and sequence tag data (see inset). Arrows indicate major fragment peaks that can be used in a database search.

The electrospray mass spectrum in Fig. 3.5 demonstrates the advantage of analyzing more than one charge state from the charge distribution. This figure shows the MS/MS spectrum from the +7 charge state of the MS2 viral coat protein and provides sequence information from a different portion of the protein. This information is complementary to that obtained from the +8 charge state and aids in database searching. When the sequence information from the MS/MS spectra is combined with the molecular weight (determined from the ion-ion charge reduction step), the data can be used to search protein databases. In this example, when the molecular weight and sequence tag generated from the +8 charge state is searched against the ExPASy Molecular Biology Server using the TagIdent Program, two hits are returned. One of them is the coat protein for MS2 (see Fig. 3.6). When the additional sequence information from the +7 charge state is included, only the MS2 entry is returned.

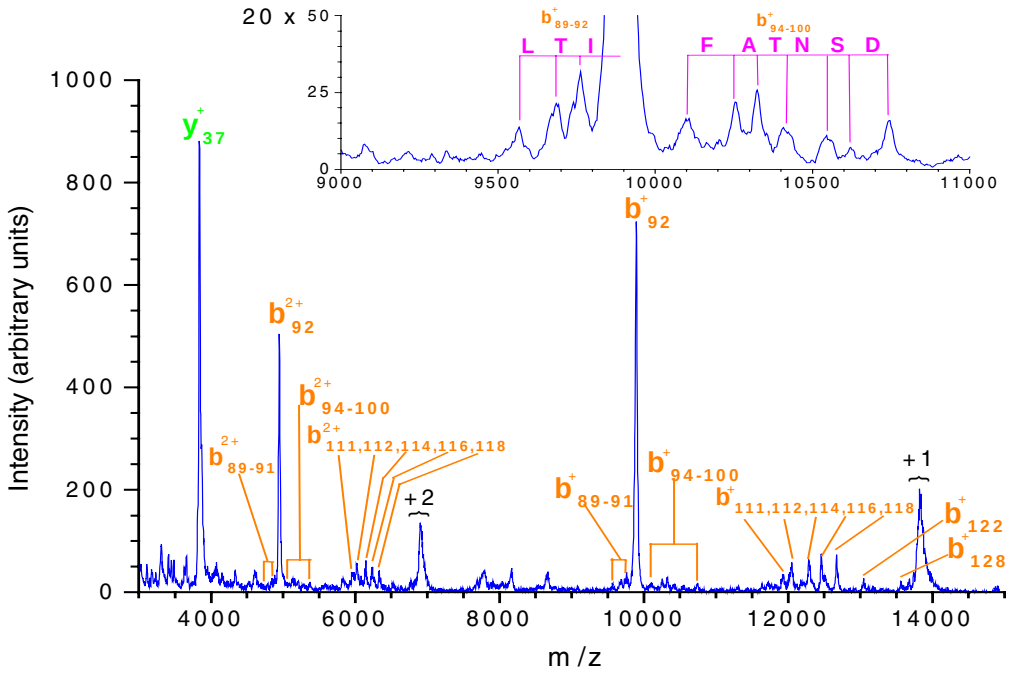

Fig. 3.5. MS/MS of the +7 charge state of the viral coat protein of MS2 showing primary fragments and sequence tag data (see inset).

COAT_BPMS2 (P03612)
COAT PROTEIN.
pI: 8.00, MW: 13728.54
105
...LTIPIFATNSDCELIvkamqgLLKDGNPIPSAIAANSGIY
COAT_BPR17 (P03613)
COAT PROTEIN.
pI: 8.67, MW: 13727.56
105
...LTIPIFATNSDCELIvkamqgLLKDGNPIPSAIAANSGIY

Fig. 3.6. Results of searching the ExPASy Molecular Biology Server using the TagIdent Program.

3.1.5 Conclusions

The use of ion-ion charge reduction enables a strategy for the analysis of biological threats based on the direct interrogation of whole protein ions via electrospray MS/MS. The identification of the toxin or organism is based on the determination of the molecular weight and partial amino acid sequence for specific proteins from the target organism. The use of ion-ion chemistry with an ion trap mass spectrometer's storage and mass selection capabilities allows sufficient ion manipulation to reduce the need to use up-front separations and enzymatic or chemical digestions of the protein. This method allows proteins to be rapidly identified from either on-system libraries or from established protein databases.

3.2 Testing with Environmental Matrices

In the summer of 2000 a test set of 15 samples was used to evaluate the ion-ion chemistry approach for the identification of biological agents in a series of complex matrices. A duplicate set of samples was also prepared (stored at –70ºC) for evaluation of the Block II CBMS instrument upon its return from field test at the joint field trials in Canada. The tests were designed to determine (1) whether the ion-ion chemistry approach is fundamentally better than the current U.S. Army's approach of using the ORNL-developed Block II CBMS and (2) whether the application is ready for hardware development (i.e., whether increased financial investment for hardware development is justified).

It is important to recognize that the laboratory instrument on which the development is currently taking place is not adequately optimized for sensitivity. In fact, most commercial instruments perform at a significantly greater sensitivity level (approximately 10 to 100 times greater) than our current prototype system. Unfortunately, these commercial instruments are not fieldable and do not have the necessary ion-ion capability needed for this application. The limitations that characterize the current laboratory-based instrument are known, and improved capabilities will be developed into the fieldable instrument. Therefore, the *ultimate* sensitivity of the technique should not be judged by this test. The broadly applicable sample-processing and introduction scheme should also be excluded from evaluation because this area is only in the early stages of investigation. The path to automate the individual sample-treatment steps is relatively clear and, in many cases, has been demonstrated elsewhere. The main goal is to validate the analytical approach, not the final instrumental implementation.

3.2.1 Experimental Details

3.2.1.1 Selection of Matrices

Three different types of matrices were selected for the initial test sequence. The first matrix, tap water, was selected to represent a possible terrorist attack on the public water supply. Possible interferences associated with this type of matrix include reducing agents, metal salts, and residual organic molecules. The second and third matrices, water from a running stream and soil, represent complex environmental matrices. They were chosen to represent the possible dissemination of an aerosolized biological release where the individual particles have solubilized in the creek or have settled on the surface of the soil.

3.2.1.2 Selection of Biological Targets

Two toxins and one virus were selected for the test procedure. Selection of the toxins was based on the molecular weight of the individual components. Melittin or bee venom has a molecular weight of 2835 Da, and cholera toxin is a five- to seven-subunit protein composed of one A-chain and four to five B-chains with an approximate molecular weight of 86 to 109 kDa. Melittin is of particular interest because this potent low-molecular-weight toxin should appear in the chemical background noise associated with the test matrices. The B-chain subunit of cholera toxin at 11.6 kDa was chosen for

detection in these experiments because of its relative abundance compared with the A-chain and because of its preferential response in an electrospray ionization experiment. The toxins were obtained from Sigma Chemical Company and were used without further purification. Both toxins were used in standard stock solutions for dilution into the various matrices. The virus MS2 was chosen for analysis as a representative viral pathogen and as a representative of the Dugway Proving Ground test mixture. Bacterial samples were not prepared at this time because we were still evaluating the protein identification procedures via ion-ion chemistry for these relatively complex organisms.

3.2.1.3 Matrix Collection

Tap water was collected at Oak Ridge National Laboratory (ORNL) from the main sink in room 104 of Building 5510. This water source is classified as nonpotable. A 35-mL sample was obtained and was stored in a 50-mL conical centrifuge tube at –70ºC.

Creek water was collected from White Oak Creek located about 35 m from Building 5510 on the ORNL site. A 35-mL sample of water and sediment was stored in a 50-mL conical centrifuge tube at –70ºC.

A soil sample was collected about 10 m to the north of Building 5510. Sample volume was measured at approximately 40 mL. Contents were primarily red clay, gravel, and small plants. This sample was also placed in a 50-ml conical centrifuge tube and stored at –70ºC.

3.2.1.4 Preparation of Samples

For the 15 samples run in each test, three sets of five 500-µL centrifuge tubes were prepared in duplicate for the three individual matrices. One 15-vial sample set was used to evaluate the electrospray ion-ion instrument. The second set was frozen at –70ºC to be run on the Block II CBMS system upon its return from Canada. Amounts of matrices used for each sample are shown in Table 3.1.

Table 3.1. Test sample matrix composition

Sample number	Amount	Toxin/virus spike
	Tap water	
1	50 µL	Blank
2	50 µL	Melittin 100 nM
3	50 µL	Melittin 1 nM
4	50 µL	Cholera toxin 1 µM
5	50 µL	Bacteriophage MS2
	Creek water	
6	50 µL	Blank
7	50 µL	Melittin 100 nM
8	50 µL	Melittin 1 nM
9	50 µL	Cholera toxin 1 µM
10	50 µL	Bacteriophage MS2
	Soil/red clay	
11	26.29 mg	Blank
12	9.37 mg	Melittin 100 nM
13	13.82 mg	Melittin 1 nM
14	25.56 mg	Cholera toxin 1 µM
15	13.29 mg	Bacteriophage MS2

Stock solutions of the various toxins were spiked into the various matrices listed in Table 3.1 to give the final concentrations listed. The concentration of the MS2 coat protein (approximately 500 nM final concentration in the sample) is estimated from an original plaque-forming unit calculation on the original

culture. The stock MS2 solution was grown in May 2000 and was placed in a nonsterile 50-mL centrifuge tube. Therefore, in addition to the media broth used to grow the culture, any other organisms present in the broth that could have grown up in a 4-month period were also present in the background. The MS2 stock-spiking solution was prepared by adding two parts glacial acetic acid to one part MS2 stock. The resulting precipitate (nuclear material) was centrifuged at 10,000 × g for 10 min, and the supernatant was used to spike the appropriate matrix samples.

Fresh extraction buffer was prepared on the day of analysis. This buffer consisted of 6-mM dithiothreitol for the reduction of disulfide bonds, 100-mM tris buffer at pH 8.0 to ensure the proper pH for the formation of the thiolate anion in the reduction process, and 8-M guanidine HCl for denaturation of proteins and solubilization of bacterial membranes (gram negative).

For the tap water and creek water samples, 50 µL of buffer was added for a total volume of 100 µL. For soil samples, 100 µL of the extraction buffer was used. The samples were then heated at 90ºC for 5 min in a heating block to facilitate the extraction/reduction process. Samples were then placed in a microcentrifuge at 2500 × g for 1 min. The supernatant was then dialyzed against a 3500-MW cutoff microdialysis membrane for 1 h. The time associated with the dialysis step is very dependent on the surface area (dialysis membrane) to volume (sample) ratio. In an automated on-line setup, this process typically takes just a few minutes.

Because the molecular-weight cutoff of the dialysis membranes exceeds the molecular weight of the melittin, 10-µL pipette tips containing a small amount of c_{18} reverse-phase packing material with a total protein binding capacity of 1 to 2 µg were used to extract the sample. The procedure used included the following steps:

1. add trifluoroacetic (TFA) acid to the sample at 0.1%,
2. wet the packing material with two volumes (10 µL) of 50:50 acetonitrile:water,
3. rinse the packing material with two volumes of 0.1% TFA,
4. pipet sample over bed volume three to five times,
5. wash captured material three to five times with 0.1% TFA, and
6. elute into 10-µL volume of 50:50 acetonitrile:water 50:50.

To the dialyzed melittin and cholera toxin B chain samples, glacial acetic acid was added to 1% (V/V ratio). To the MS2 samples, glacial acetic acid was added to 66% (V/V) to prevent coagulation of coat protein molecules.

A summary of the sample preparation steps can be seen in Table 3.2. A 10-µL aliquot of each sample was then analyzed directly via electrospray ion trap ion-ion mass spectrometry.

Table 3.2. Sample preparation steps

Bacteriophage MS2, cholera		**Melittin**	
Sample step (dialysis)	**Time required (min)**	**Sample step (concentration)**	**Time required (min)**
Add extraction buffer	0.1	Add extraction buffer	0.1
Vortex	0.5	Vortex	0.5
Heat to 95°C	5.0	Heat to 95°C	5.0
Microcentrifuge	1.0	Microcentrifuge	1.0
Microdialysis	60.0	C_{18} preconcentration	5.0
Add acetic acid 1%	0.1	Add acetic acid 1%	0.1
Remove 10 µL for MS	0.1	Remove 10 µL for MS	0.1

3.2.2 Electrospray Ion Trap Ion-Ion Mass Spectrometry of Toxin/Viral Protein Standards

Several days prior to sample analysis, standard solutions of melittin (10 μM) and cholera toxin B-chain (10 μM) were analyzed and were used as standard data for direct comparison with the matrix samples. Because we have extensive experience with bacteriophage MS2, the data published in our most recent paper was used as the comparison standard (Cargile et al. 2000).

Figure 3.7 shows the electrospray mass spectrum of melittin. The primary peak observed is that of the +4 charge state. This will be the target ion for analysis of the toxin. Figure 3.8 shows the mass isolation of the +4 charge state of melittin. All other ions are ejected from the trap (compare to the spectrum in Fig. 3.7). Therefore, if a significant peak is detected in the mass isolation spectrum, then MS/MS analysis is performed.

Figure 3.9 shows the ion-ion reaction mass spectrum derived from MS/MS fragmentation of the +4 charge state of melittin. The most intense product ion arises from the commonly observed cleavage at proline, which is the peak labeled y_{13}, where y_{13} (amide bond cleavage Leu^{13}-Pro^{14}) refers to a fragment ion that is 13 amino acid residues long counting from the c-terminus. In this example, potential charge state overlap is eliminated in the m/z region greater than half the mass of the singly charged parent ion. All ions appearing in this region must be singly charged. Charge state overlap is still possible below half-mass. However, when the reaction time is chosen to yield primarily singly charged ions, there should be no doubly charged ions without a singly charged ion also present in the mass spectrum. This greatly facilitates the identification of the doubly charged ions in the mass spectrum.

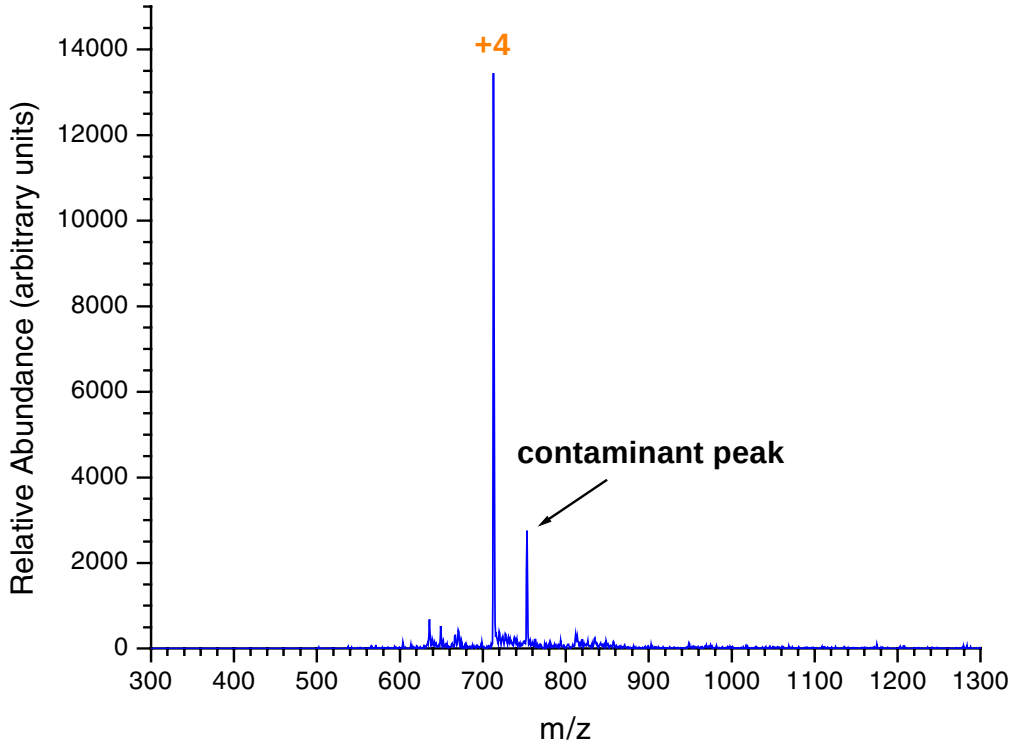

Fig. 3.7. Electrospray mass spectrum of the toxin melittin showing primarily the +4 charge state and one contaminant peak.

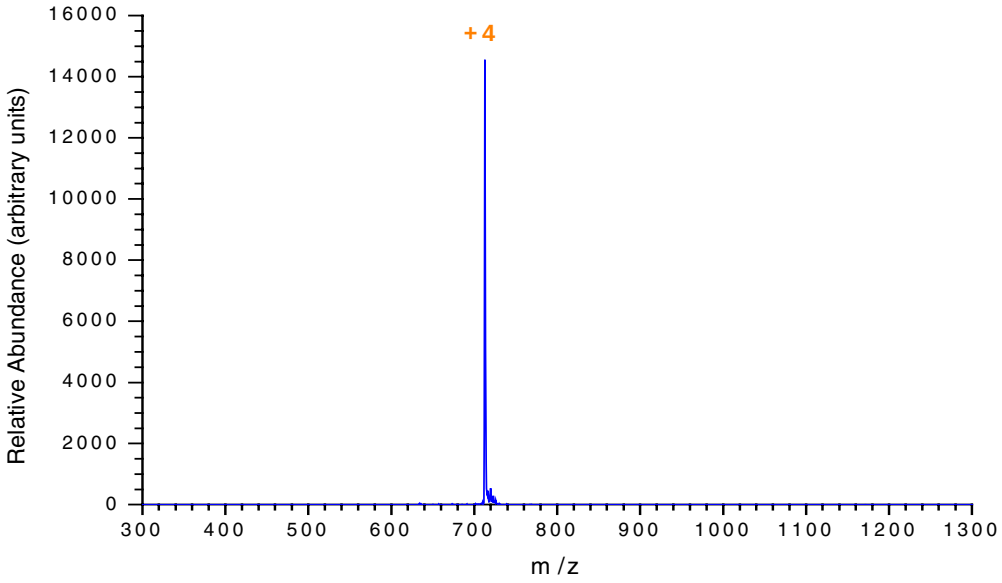

Fig. 3.8. Mass isolation of the +4 charge state of melittin.

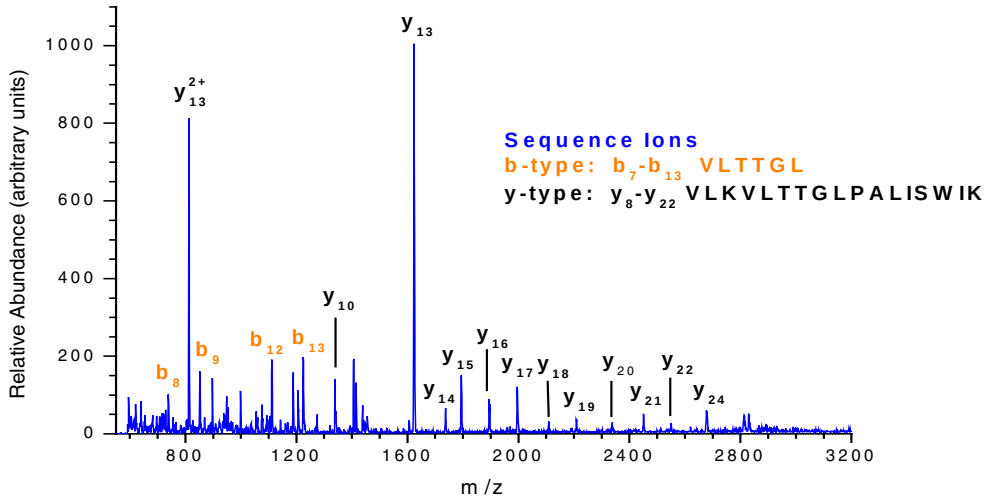

Fig. 3.9. MS/MS post-ion-ion reaction mass spectrum derived from the +4 charge state of melittin. The major b- and y-type ions are labeled.

The signal level of the y_{13} product ion dominates the MS/MS post–ion-ion reaction mass spectrum; however, signals can be readily identified for the b-series ions b_7–b_{13} (Val-{Leu/Ile}-Thr-Thr-Gly-{Leu/Ile}, counting amino acid residues from the n-terminus) and for the y-series ions y_8–y_{22} (Val-{Leu/Ile}-{Lys/Gln}-Val-{Leu/Ile}-Thr-Thr-Gly-{Leu/Ile}-Pro-Ala-{Leu/Ile}-{Ile/Leu}-Ser-Trp-{Ile/Leu}-Lys), and y_{24}. The large degree of fragmentation observed with the +4 charge state of melittin provides several options for detection and identification strategies. Effective strategies for unambiguously

identifying target protein toxins are matching an MS/MS library spectrum, generating a sequence tag, or performing a database search on the most intense product ions by using the basic rules of intact protein fragmentation derived by our initial studies. The data from the melittin experiments are designed to test the sequence tag approach to protein toxin identification in real-world matrices.

Figure 3.10 shows the electrospray mass spectrum of the cholera toxin B-chain standard. The +9 charge state ion (m/z 1291, Fig. 3.11) is used as the trigger for the MS/MS experiment. The MS/MS post-ion-ion reaction mass spectrum is shown in Fig. 3.12. The same approach to recognizing singly charged vs doubly charged ions for melittin is also used for interpreting the cholera toxin B-chain MS/MS data. The most intense ion produced in the product ion spectrum is the loss of a c-terminal asparagine to form a b_{102} ion. Subsequent adjacent fragmentation to form the b_{97}–b_{102} series (Ala-{Ile/Leu}-Ser-Met-Ala-Asn-COOH) is also observed. Interestingly, this series of product ions does not follow some of the basic rules of intact protein fragmentation observed in our laboratory. At this time we have no explanation for this phenomenon, and we decided to use this toxin as a test compound due to the inherent differences associated with the fragmentation of cholera toxin B-chain compared with those of other toxins/viruses analyzed in our laboratory. Therefore, because the MS/MS data generated for the +9 charge state of cholera toxin B-chain yield primarily a small series of sequence-specific ions near the c-terminus, this toxin is used to test the library search approach to protein identification in the presence of complex sample backgrounds.

The standard MS/MS post-ion-ion reaction mass spectrum of the +8 charge state of the bacteriophage MS2 coat protein is shown in Fig. 3.13. For this test, the +8 charge state was used as the trigger to MS/MS experiment. The data shown in Fig. 3.13 were obtained from the analysis of viral coat proteins via ion-ion chemistry (Cargile 2000). The major peaks observed in the MS/MS spectrum of the +8 charge state are b_{118} (Ile^{118}-Pro^{119}), b_{116} (Asn^{116}-Pro^{117}), and b_{92} (Ile^{92}-Pro^{93}), which correspond to cleavages on the n-terminal side of proline. Extensive fragmentation at adjacent amino acid residues is observed in the region of the b_{116} ion. The b-type ion series ranging from b_{104} to b_{116} yielded an amino acid sequence tag of 12 residues (Val-{Lys/Gln}-Ala-Met-{Gln/Lys}-Gly-{Leu/Ile}-{Leu/Ile}-{Lys/Gln}-Asp-Gly-Asn).

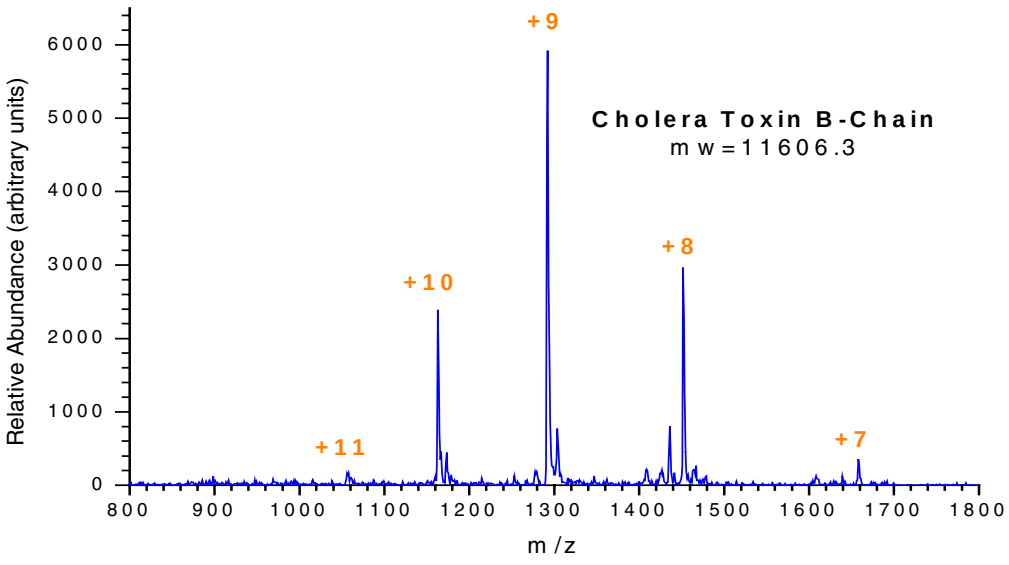

Fig. 3.10. Electrospray mass spectrum of cholera toxin B-chain.

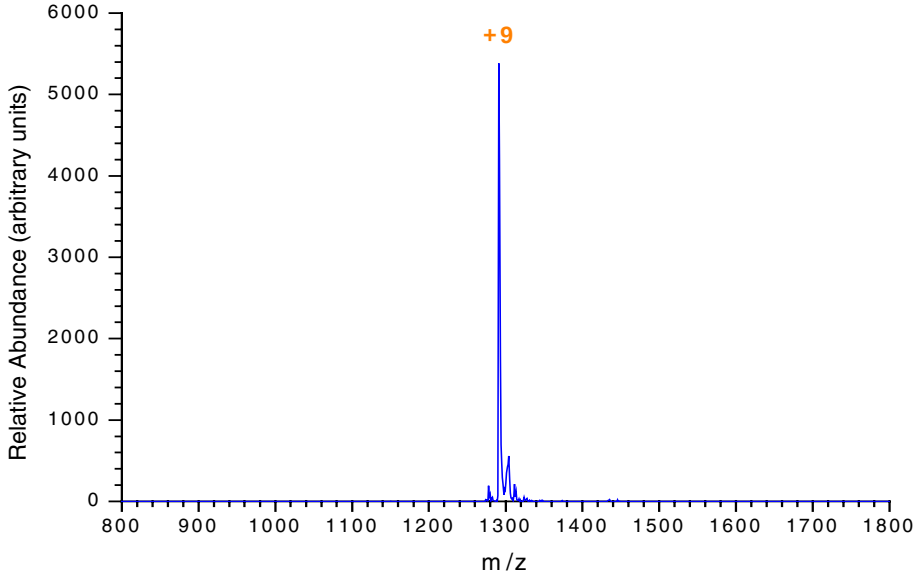

Fig. 3.11. Mass isolation of the +9 charge state from cholera toxin B-chain.

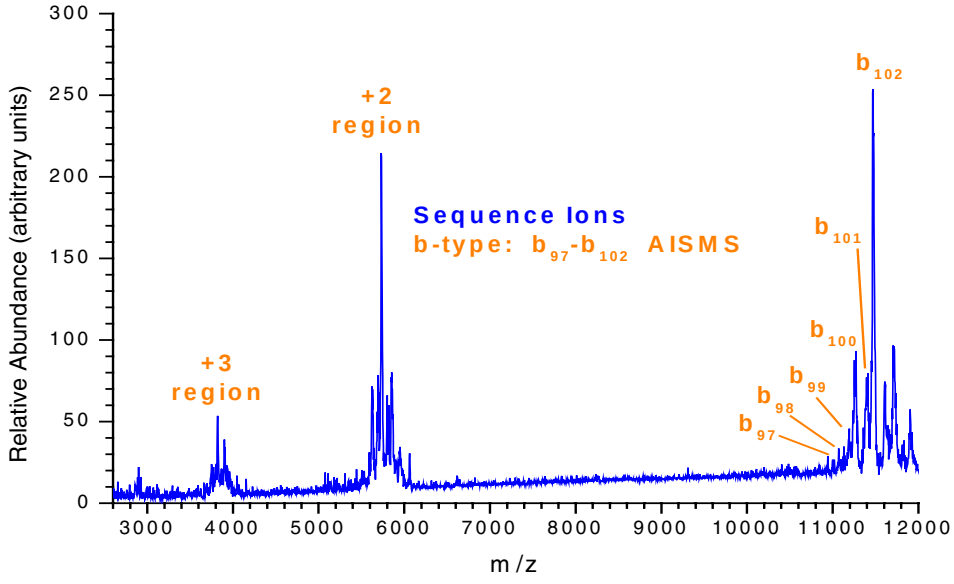

Fig. 3.12. MS/MS post-ion-ion reaction data for the +9 charge state of cholera toxin B-chain.

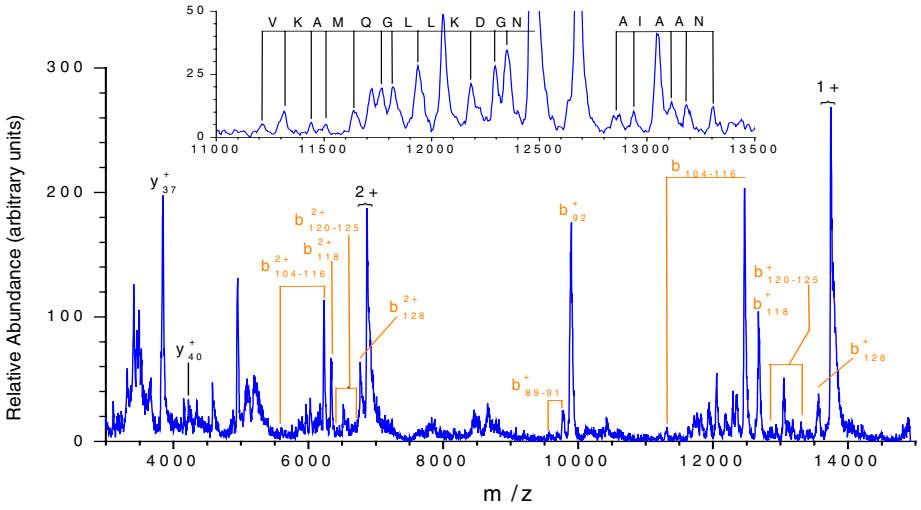

Fig 3.13. MS/MS post-ion-ion reaction mass spectrum derived from the +8 charge state of the MS2 coat protein. Insert contains an expanded view of the region between m/z 11,000 and 13,500.

In addition, fragmentation at adjacent residues occurs in the b_{122} ion region for the MS/MS data of the +8 charge state. This small series of cleavages $b_{122–125}$ (Ala-{Ile/Leu}-Ala-Ala-Asn) at adjacent residues is of particular interest because the prominent peak in the series, b_{122}, represents cleavage between two alanine residues, and not the usual n-terminal proline or c-terminal acid residue fragmentation typically associated with the most intense ions derived from the MS/MS of intact proteins. Although the MS/MS analysis of this charge state produces a rich array of sequence tag data, the algorithm developed in our laboratory for analysis of intact proteins (based on the fragmentation rules from our previous work) is used to identify the presence of the MS2 coat protein in the various matrices.

3.2.3 Electrospray Ion Trap Ion-Ion Mass Spectrometry for the Analysis of the Test Samples

A series of three preprogrammed analysis routines for melittin, cholera toxin B-chain, and the MS2 viral coat protein were set up on the control computer for the ion-ion instrument. These preprogrammed routines were based directly on the results obtained from the standard analysis described in Sect. 3.2.2. The basic steps of the melittin and cholera toxin B-chain routines included an initial ion accumulation step (20–200 ms), mass isolation (60–90 ms), MS/MS (250–750 ms), anion injection (20 ms), mutual storage/reaction time (100 ms), and mass analysis step (110 ms). The total instrument scan time ranged from 560 to 1270 ms (approximate times). Each data file consisted of an average of 3 to 20 scans, depending on the type of data collected (e.g., MS/MS-ion-ion, mass isolation, electrospray only). Also, for each sample anywhere from 5 to 20 data files were collected, depending on the signal-to-noise ratio for each analysis.

For each sample and standard analyzed, a 10-µL aliquot was pipetted into a 1.5-mm-OD borosilicate glass capillary with a tapered “needle” orifice having a diameter between 3 and 8 µm. The glass capillary was then inserted into a microelectrode holder modified with a tungsten wire for electrical contact. The positive potential applied to the solution ranged between 800 and 1300 V.

3.2.4 Results and Discussion

3.2.4.1 Tap Water Matrix

Figure 3.14 shows the electrospray mass spectrum of a tap water matrix sample. The primary background observed is that of a small baseline lift-off between m/z 600 and m/z 1600. These results are not surprising because most background contamination is presumably due to small inorganic and organic species, which are readily eliminated by the microdialysis step of the sample preparation procedure.

The post-ion-ion reaction mass spectrum of the tap water matrix is seen in Fig. 3.15. For this sample no discrete peaks were observed up to m/z 12,000. The relatively low background seen in the mass spectrometer for this matrix allows for direct mass isolation and dissociation of various toxin samples, followed by charge reduction to primarily the +1 charge state.

For sample numbers 2 and 3, which contained 100 nM and 1 nM, respectively, of the toxin melittin, both samples were easily characterized by their signature MS/MS post-ion-ion reaction mass spectra, whereby a sequence tag could be easily obtained. Figure 3.16 shows the post-ion-ion reaction mass spectrum derived from sample 3 (1-nM melittin toxin in tap water). The sequence tag VLKVLTTGL was easily read from the y_{13} ion to the y_{22} ion, thus confirming a positive identification for the melittin toxin.

Sample number 4 was spiked to a 1-µM concentration of cholera toxin, which could also be easily identified in the tap water matrix. By matching the post-ion-ion reaction mass spectra derived from the standard to that of the sample shown in Fig. 3.17, the presence of cholera toxin can be confirmed. The presence of the three most intense fragments, which represent cleavage at the c-terminal end of the protein, are readily apparent in Fig. 3.17 and therefore could be library-searched against the standard spectrum shown in Fig. 3.12.

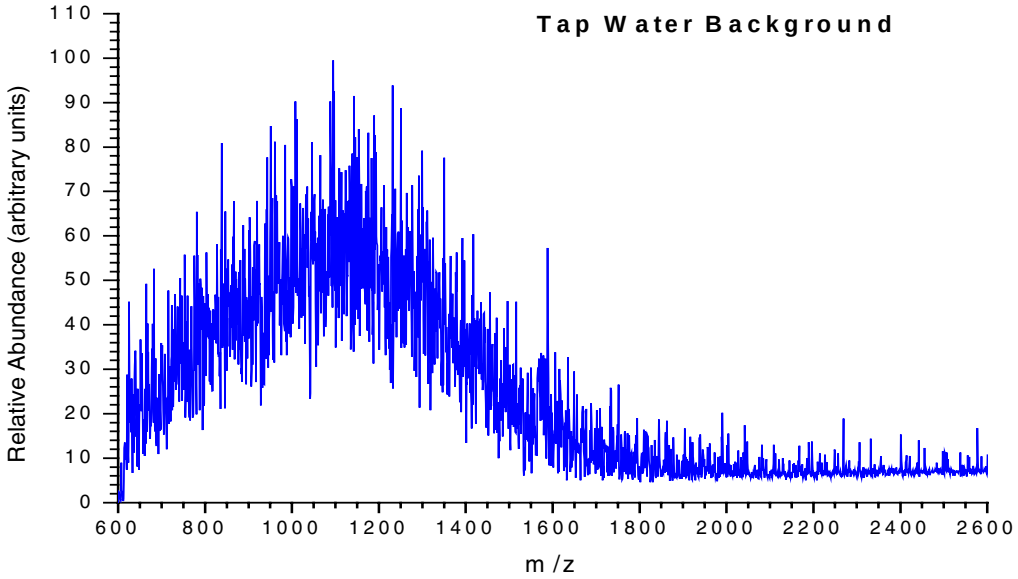

Fig. 3.14. Electrospray mass spectrum of tap water matrix showing a small baseline lift-off between m/z 600 and 1600.

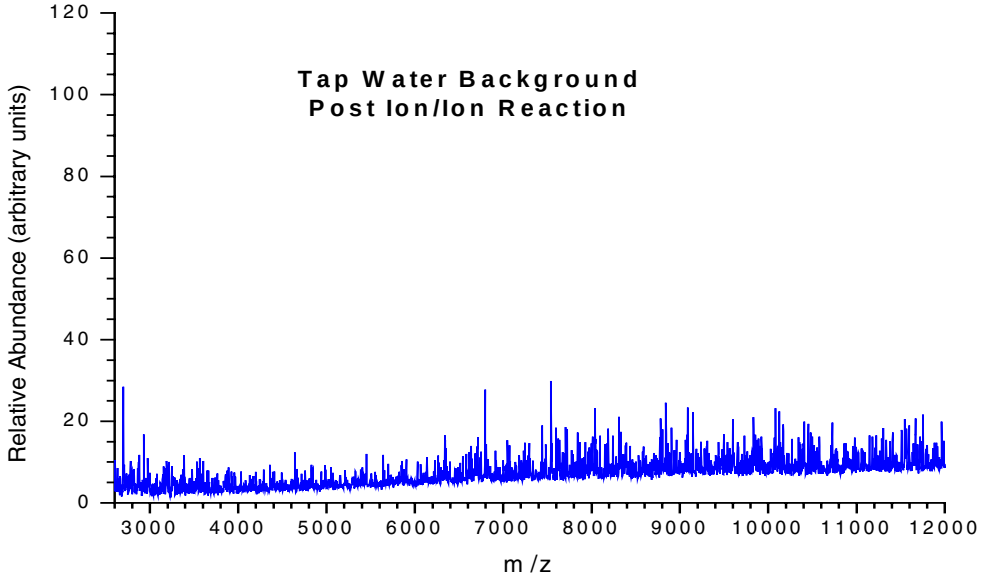

Fig. 3.15. Post-ion-ion reaction mass spectrum derived from tap water matrix.

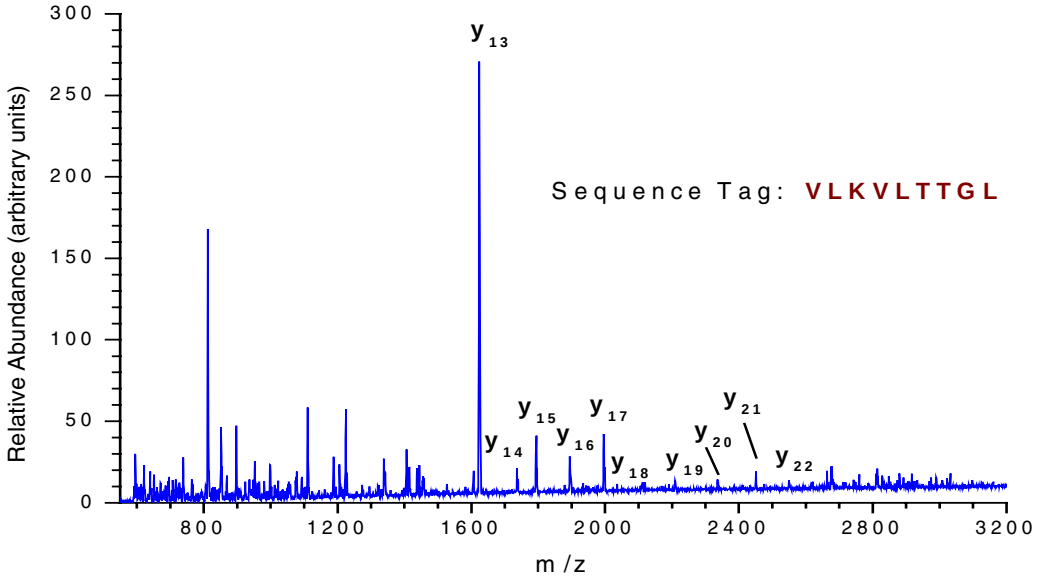

Fig. 3.16. Post-ion-ion reaction mass spectrum of sample 3 showing the sequence tag VLKVLTTGL.

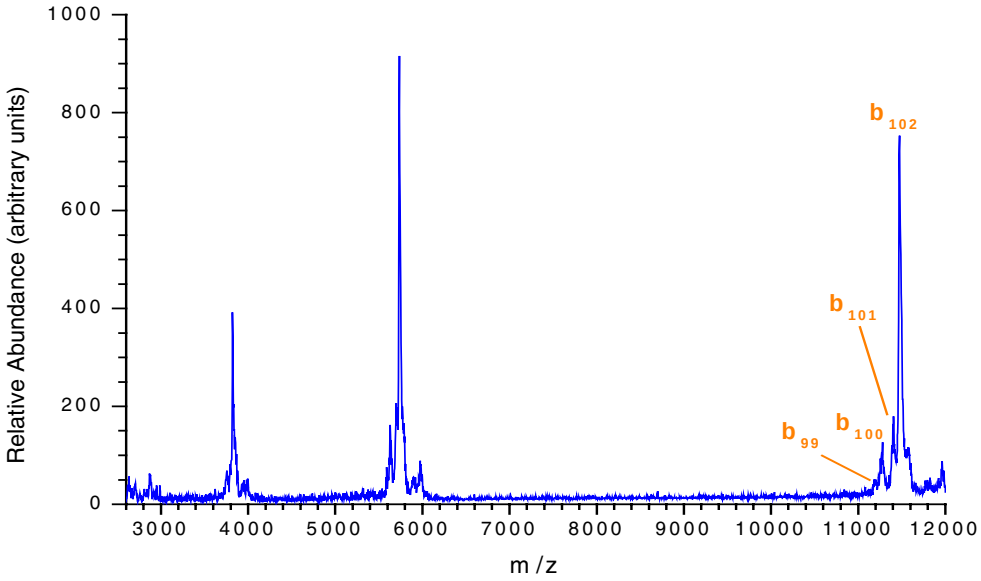

Fig. 3.17. Detection of 1-µM cholera toxin in a tap water matrix.

3.2.4.2 Creek Water Matrix

Figure 3.18 shows the electrospray mass spectrum of a creek water matrix sample. The intensity of the background associated with this sample is approximately 15 times greater than that of tap water. In addition, several prominent peaks are present between m/z 700 and m/z 1200. The baseline lift-off for this sample ranges between m/z 600 and 3000 and shows a series of discrete peaks at about three times the signal-to-noise ratio between m/z 2000 and m/z 2600. Because the goal of this test was to evaluate the system for toxin and virus analysis, no specific effort was directed toward determining the identity of these individual components.

Figure 3.19 shows the post-ion-ion reaction mass spectrum of the creek background matrix. A series of evenly spaced peaks observed between m/z 2600 and m/z 6000 is seen in this post-ion-ion reaction mass spectrum, indicating the possible presence of detergent(s). Detergents could interfere with the MS/MS data generated for toxin identification and can easily suppress the electrospray ionization process. It is also evident from this data that an improved microdialysis experiment would be needed to address this problem.

Melittin samples (sample numbers 7 and 8) at 100 nM and 1 nM were analyzed with the creek matrix. The 100-nM sample was easily detected with the sequence tag VLKVLTTGL, as seen in Fig. 3.20. However, with the melittin samples the preparation method involved preconcentration by using a C_{18} reverse-phase packing material that discriminates effectively against any detergent present in the matrix. Microdialysis cassettes were not used for these samples due to the molecular weight cutoff of the membrane at 3500, which is greater than the molecular weight of the toxin. For the 1-nM sample, the mass isolation step produced a precursor peak with a limited signal-to-noise ratio whereby identification via MS/MS and ion-ion chemistry would not be possible (see Fig. 3.21).

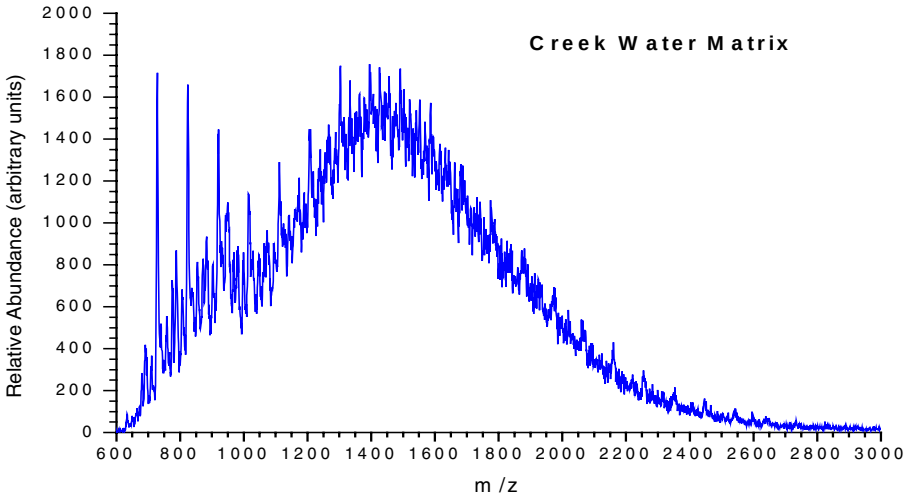

Fig. 3.18. Electrospray mass spectrum of the creek water matrix. Several discernable unknown peaks are present between m/z 700 and 1200.

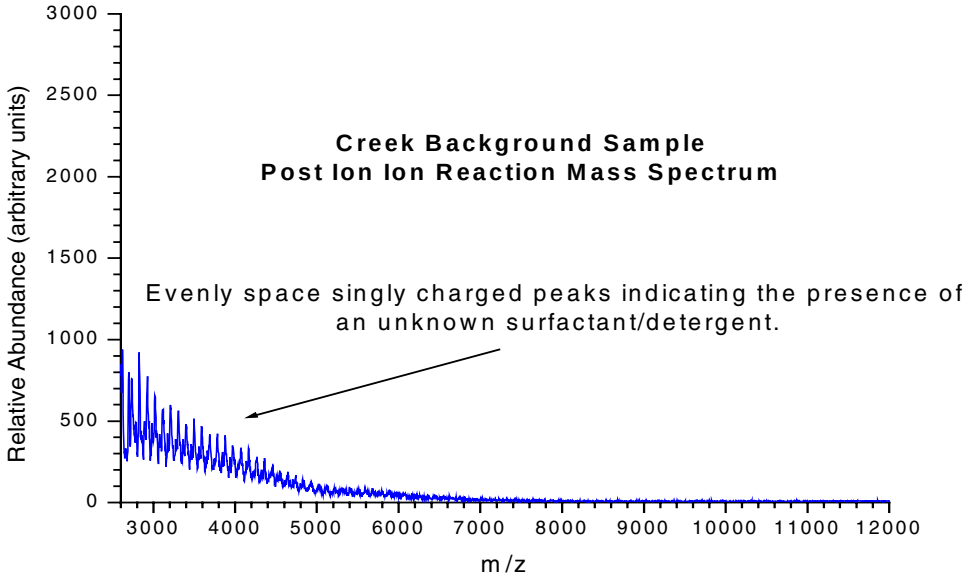

Fig. 3.19. Post-ion-ion reaction mass spectrum of the creek water matrix showing the presence of a possible detergent.

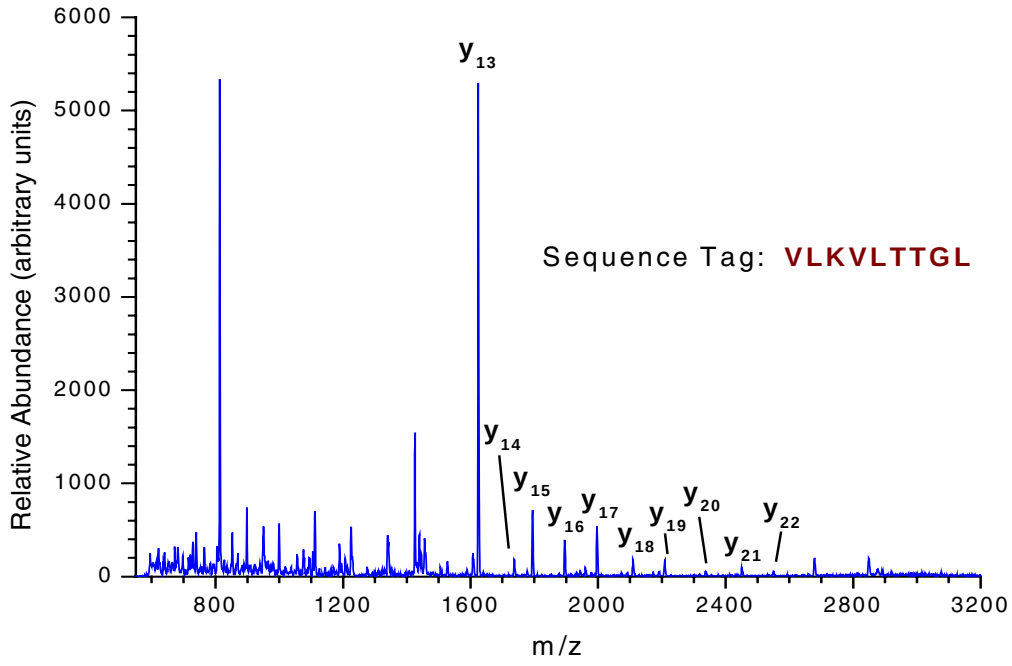

Fig. 3.20. Detection of melittin in the creek water matrix using a c_{18} preconcentration step.

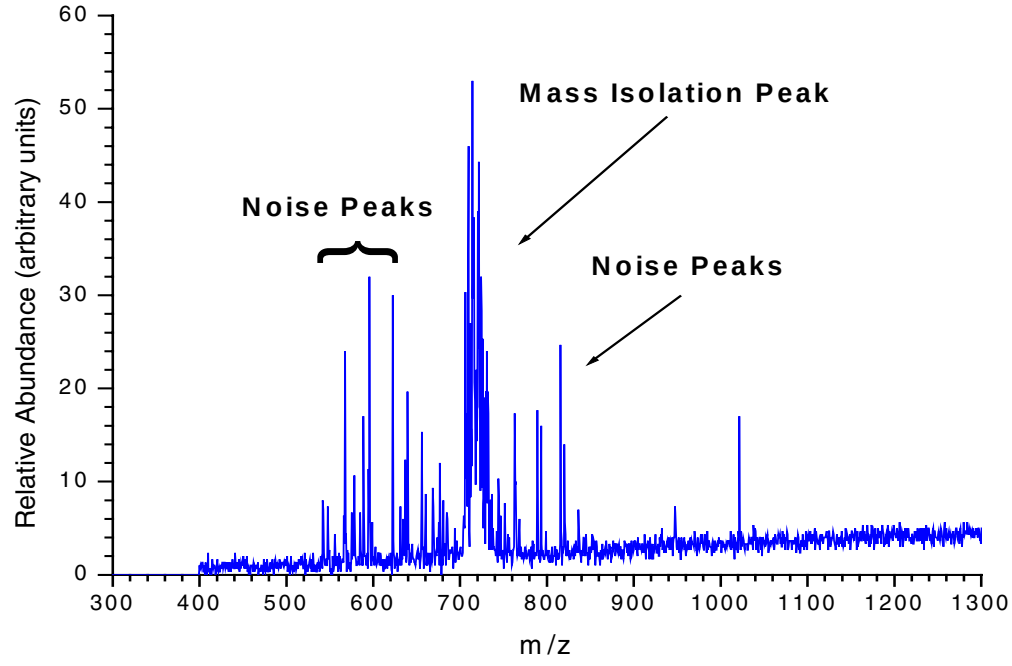

Fig. 3.21. Mass isolation of the +4 charge state of melittin from the 1-nM spike in the creek water matrix.

Sample number 9 containing the cholera toxin at a concentration of 1 µM could not be analyzed successfully under any electrospray mass spectrometry conditions. No stable signal could be obtained at any of the interface settings used. To determine whether proteolytic enzymes could be responsible for the lack of signal, an additional spike of cholera toxin was added to the sample to bring the sample concentration to 2 µM. Even in that case, no stable signal could be obtained, which suggests that matrix effects and not proteolytic enzymes from lysed bacteria are the cause of the unstable signal. However, after performing a concentration step using the c_{18} reverse-phase packing material, cholera toxin could be identified successfully (see Fig. 3.22).

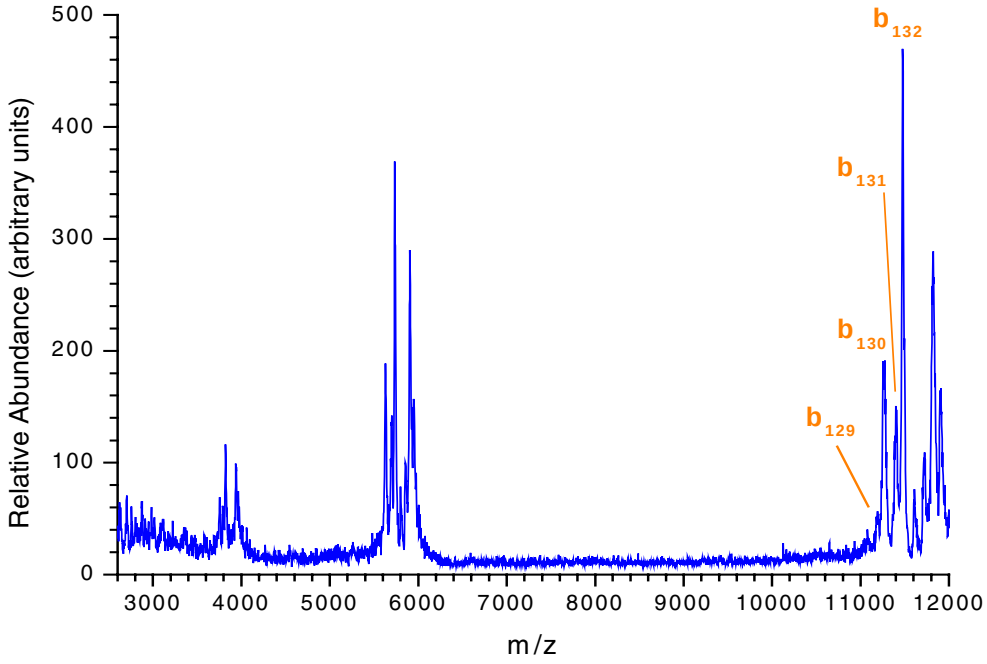

Fig. 3.22. Detection of cholera toxin in the creek water matrix after a preconcentration step using c_{18} reverse-phase material.

3.2.4.3 Soil/Red Clay Matrix

The electrospray mass spectrum of the soil/red clay matrix is shown in Fig. 3.23. This sample is characterized by a baseline rise between m/z 600 and m/z 2000 with a maximum intensity of approximately 800 counts. Also present are several discernable peaks above m/z 1600, which could be related to a bacterial species indigenous to this specific soil type. Figure 3.24 shows the post-ion-ion reaction mass spectrum of the same sample taken to primarily the +1 charge state. Five distinct singly charged ions are present between m/z 6000 and m/z 9000, which may further support our hypothesis concerning soil type biomarkers. Because the goal of these experiments was to detect a variety of toxins/viruses in a complex matrix and not to characterize environmental background, no attempt was made to identify these peaks.

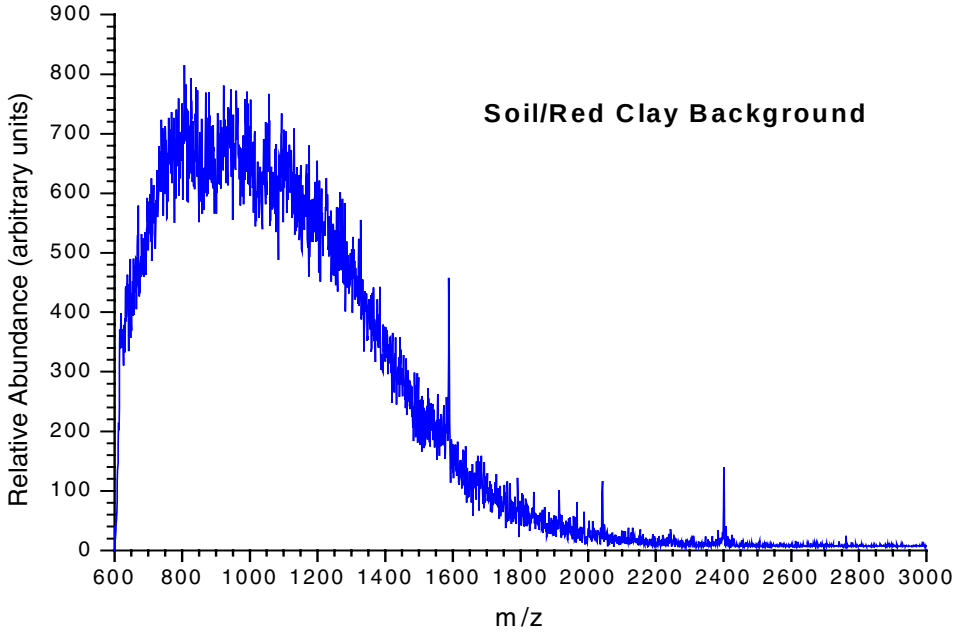

Fig. 3.23. Electrospray mass spectrum of soil/red clay background showing several discrete peaks above m/z 1600.

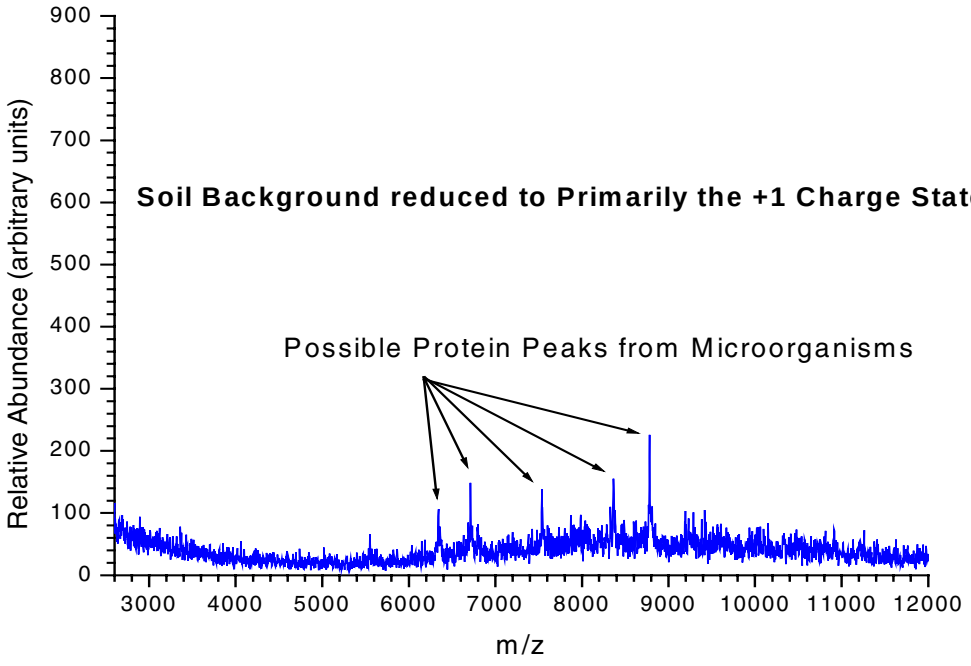

Fig. 3.24. Post-ion-ion reaction mass spectrum of the soil matrix.

For sample 12, which contained a 100-nM concentration of melittin, the presence of the VLKVLTTGL sequence tag confirmed the presence of this toxin in the soil/red clay matrix. For the corresponding 1-nM sample (sample number 13), a partial sequence tag was obtained at the signal-to-noise level of the experiment, as shown in Fig. 3.25. In this example, the partial tag obtained was VLKV, which corresponds to the y-series of y_{13}–y_{17}. Additional fragment ions consisting of y_{19} and y_{21} were also observed and further confirmed the presence of melittin. Also seen in the spectrum are random signals caused by electronic noise, which could conceivably affect the spectral interpretation process for samples with low signal-to-noise ratios.

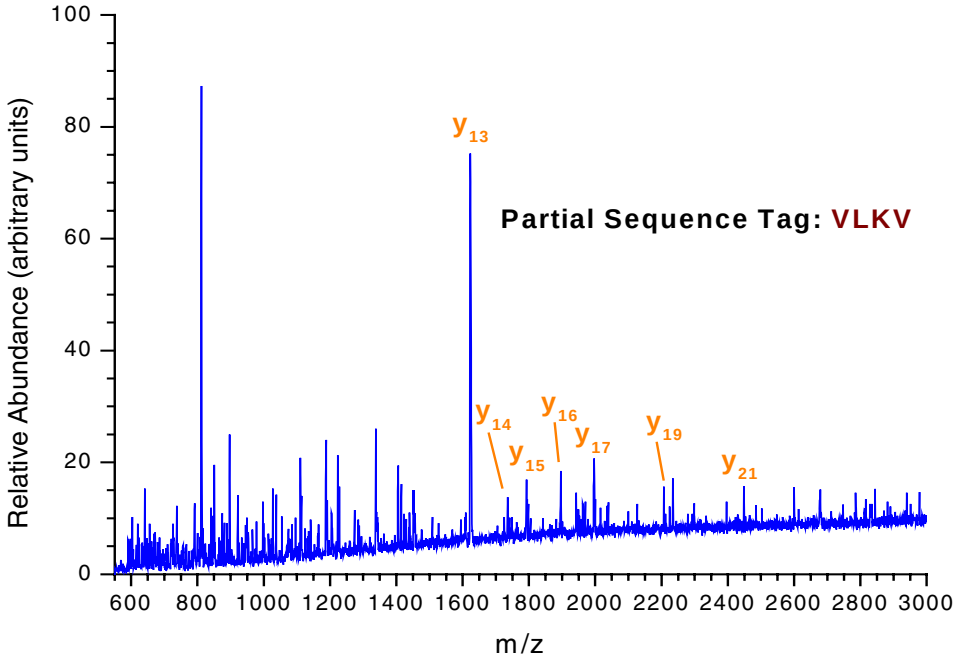

Fig. 3.25. MS/MS post-ion-ion reaction of 1-nM melittin sample showing partial sequence tag.

For the 1-µM sample of cholera toxin, a library match can be obtained easily for the data displayed in Fig. 3.26. In this example, as in previous matrices, the prominent peaks represent cleavage at the c-terminal end of the protein. Three prominent peaks between m/z 9000 and m/z 10,000 could not be identified and may be a result of the complex soil/red clay matrix.

The final series of samples analyzed contained the MS2 virus in the three environmental matrices. In the case of the creek water matrix, no stable signal was obtained under any conditions (sample 9), and therefore a positive hit could not be scored. For both the tap water and soil matrix, the immense background associated with the MS2 sample overwhelmed the background associated with each matrix. The following discussion for sample 15 (MS2 in soil/red clay matrix) applies to sample 5 as well (MS2 in tap water matrix). Figure 3.27 shows the electrospray mass spectrum of sample 15 with the corresponding charge state distribution of the MS2 coat protein superimposed on the sample background. Because the standard spectrum shown in Fig. 3.13 represents the MS/MS post-ion-ion reaction data derived from the +8 charge state, an ion-ion reaction will be needed to increase the intensity of the +8 charge state and separate the charge state of interest from the environmental background.

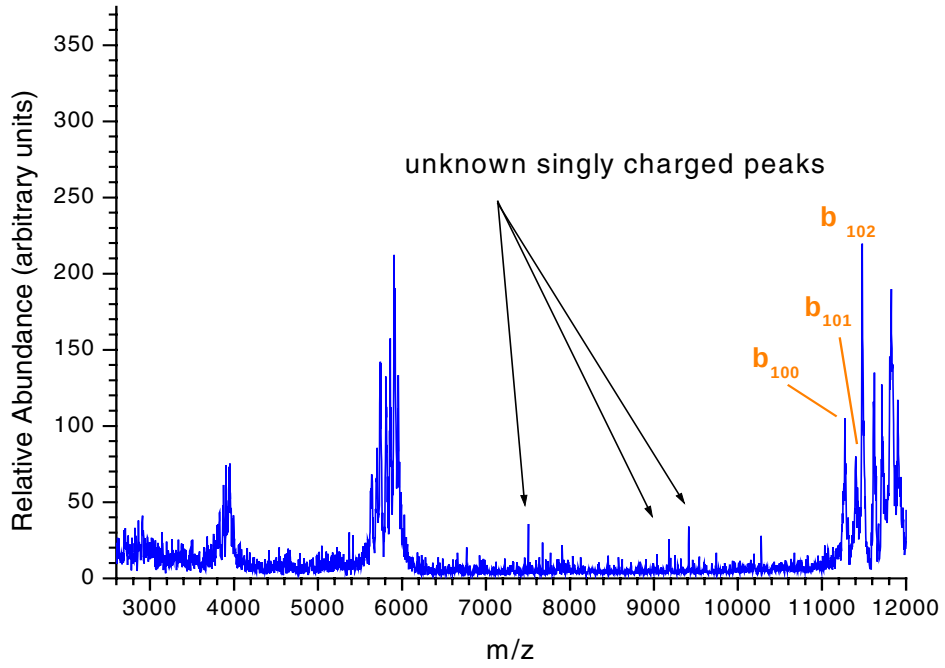

Fig. 3.26. Detection of cholera toxin in the soil matrix.

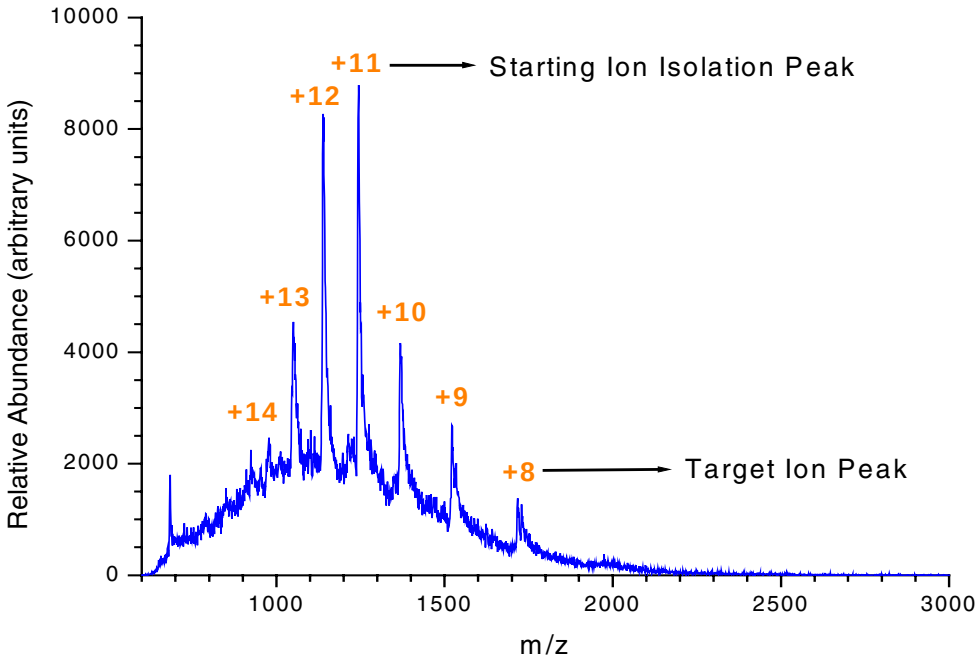

Fig. 3.27. Electrospray of MS2 spiked soil sample showing the charge state distribution of MS2 on the large background signal.

The next step of this process is illustrated in Fig. 3.28, which shows the isolation of the +11 charge state and any background ions that are at the same m/z as the precursor ion. Next is a short ion-ion reaction time followed by mass analysis. The results in Fig. 3.29 show the charge state distribution shifted to lower charge (centered on the +8 charge state), and demonstrate the utility of ion-ion reactions for sample cleanup. The remaining ion signal from the original mass isolation of the +11 charge state is that of singly charged noise, which is seen in Fig. 3.29 as a broad, ill-defined peak in the spectrum. Next, the +8 charge state is isolated, as shown in Fig. 3.30, and the final step is the MS/MS and subsequent ion-ion reaction demonstrated in Fig. 3.31. The four most intense ions in this spectrum (y_{37}, b_{92}, b_{116}, b_{118}) were used with the computer algorithm to identify unequivocally the MS2 bacteria coat protein. The major emphasis of the algorithm is on the predicted cleavage of proteins on the n-terminal side of prolines and the c-terminal side of aspartic and glutamic acid.

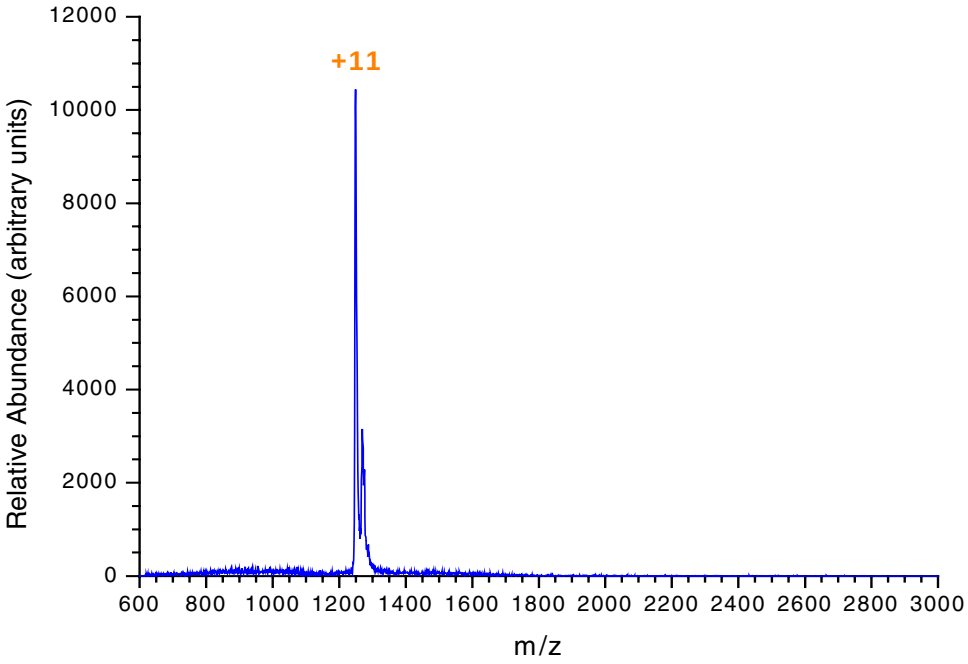

Fig. 3.28. Isolation of the +11 charge state plus the accompanying background.

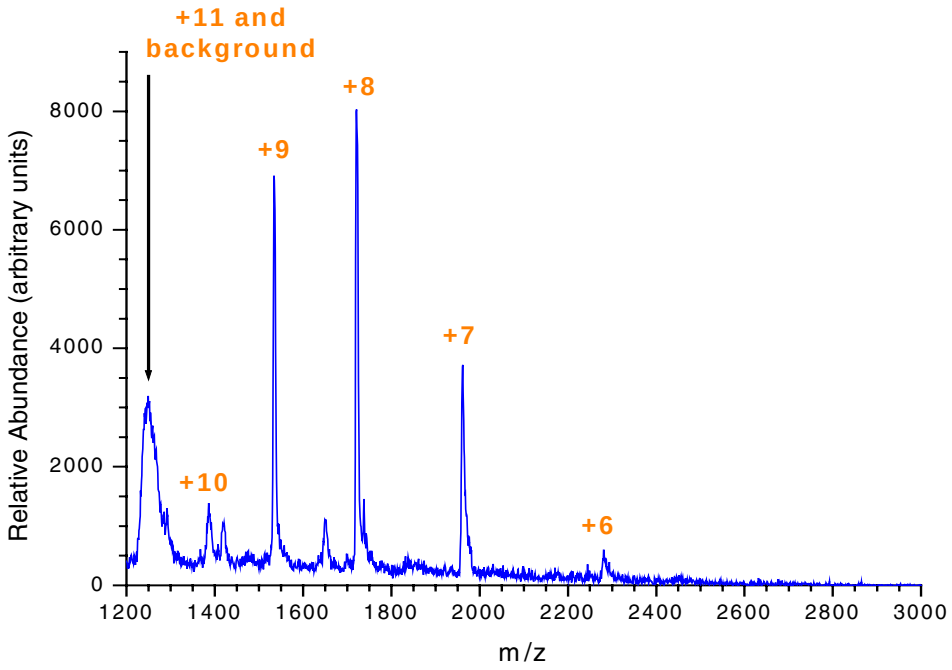

Fig. 3.29. Ion/ion reaction of the isolated +11 charge state to form the target +8 charge state used for the MS/MS experiment.

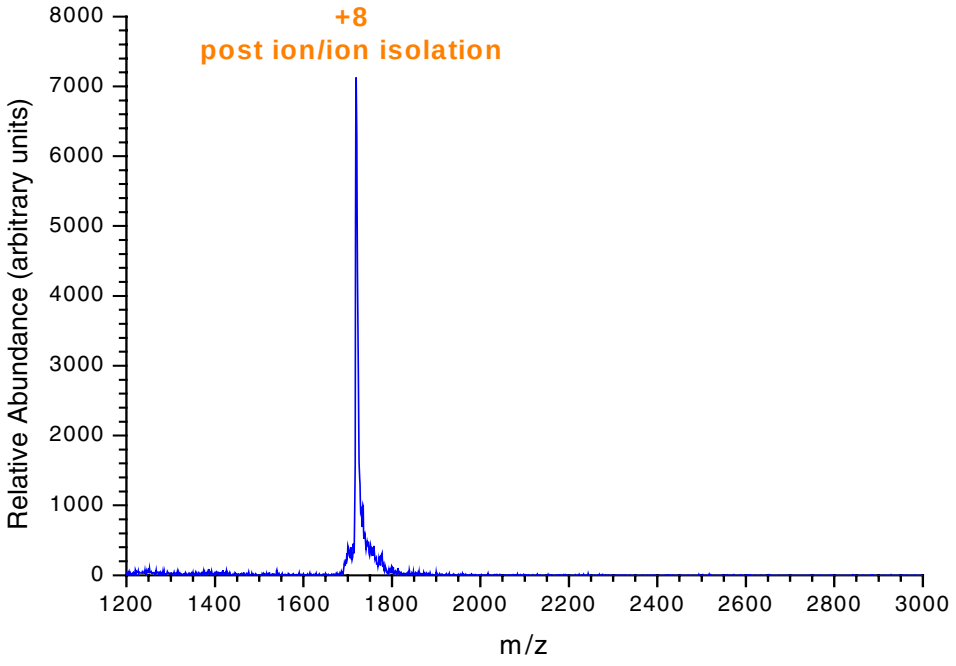

Fig. 3.30. Post-ion-ion isolation of the "purified" +8 charge state.

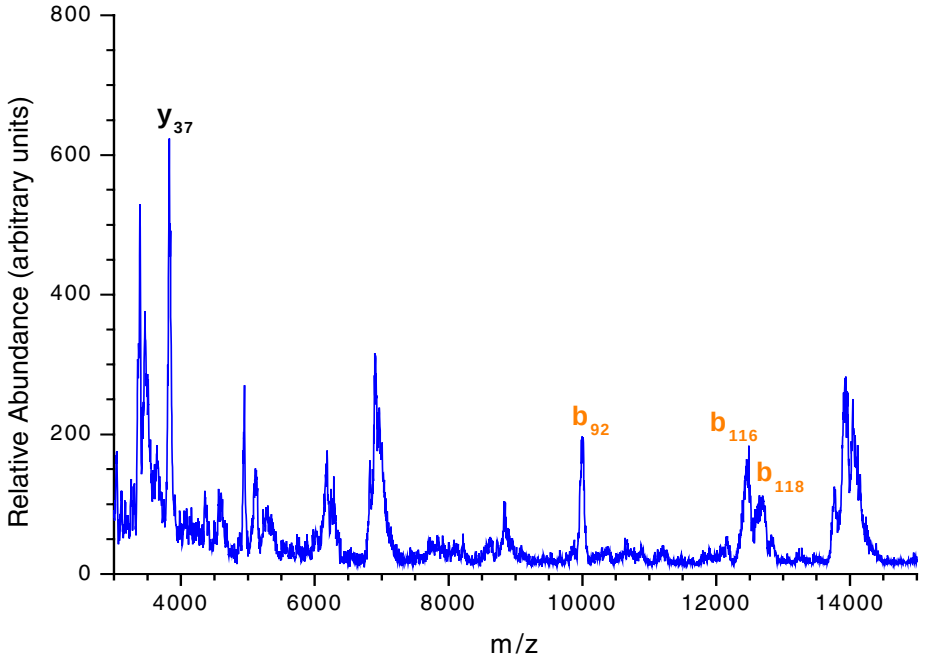

Fig. 3.31. MS/MS post-ion-ion of the +8 charge state of the MS2 coat protein in soil matrix.

Two interesting aspects of these data are the lack of sequential fragmentation seen in the standard data shown in Fig. 3.13 and the broadened peak shape of the charge-reduced product ions. This peak broadening could be due to a variety of factors, including the presence of matrix ions in the MS/MS experiment (which can affect the collisional activation conditions). In addition, the energy deposition process for the charge state of interest may not be optimal (requiring time or amplitude adjustment of the resonance excitation signal), and/or resonance ejection conditions may not be optimized for the number of ions stored in the ion trap.

3.2.4.4 Time of Analysis

Table 3.3 shows the total time of analysis needed to run an individual sample (See Table 3.2 for a summary of the sample preparation steps.). The sample preparation step is broken down into two separate categories, one for the c_{18} preconcentration step (melittin samples) and another for the dialysis step (cholera toxin and bacteriophage MS2). The approximate 12 min needed for the preconcentration step (which is manually very intensive) can be decreased significantly with appropriate microfluidics system design. In the case of the dialysis experiment, a flow-through system could be incorporated to increase the surface-area-to-volume ratio and thereby cut the dialysis time by more than an order of magnitude. The sample-loading process, which currently consists of pipetting 10 µL of sample extract into a nanospray needle, can be automated easily by using a continuous flow-through system. However, the time savings associated with this step will be minimal (currently 0.1 min).

For generating a stable electrospray system, a continuous flow design will place sufficient backpressure on the nanospray needle to make this step much more reproducible. Currently, the electrospray process is driven by electroendo-osmotic flow, which will produce a stable signal primarily for samples containing a few percent of organic solvent (which reduces the viscosity of the solution). A small amount of

Table 3.3. Sample-processing and analysis times

Procedure	Time (min)
Sample preparation	11.8 (C_{18} preconcentrate, melittin) 66.8 (dialysis, cholera and MS2)
Sample loading	0.1
Stabilize electrospray	0.1–5
Data acquisition (10 data files)	15
Data processing (file averaging, calibration)	10
Data interpretation (tags, library, algorithm)	5

backpressure derived from a continuous flow system, combined with the appropriate software control of the electrospray voltage, can overcome the aforementioned difficulties. This should reduce the time necessary (reproducibly) to 0.1 to 0.3 min.

Data acquisition is severely limited on our current system. To acquire data, we must use a 80386/80486 processor clocked at under 25 MHz that relies on a nonstandard interface card designed by Finnigan in the early 1980s. In addition, the on-board computer for the Finnigan electronics is an 80086. These limitations can be addressed by adapting our acquisition system to that used for the CBNP Block II CBMS system or to that of the current state-of-the-art ion trap system designed by Finnigan. This approach will reduce acquisition times to approximately 1 to 2 min. Our current data-processing time (shown in Table 3.3) of 10 min includes manual averaging of the 10 acquired data files in an Excel spreadsheet, plus an off-line data calibration step. With the appropriate software and acquisition hardware, this time can be reduced to several seconds. Depending on the final format employed for the advanced ion trap system (different toxins/organisms may require different interpretation algorithms), the electronic data interpretation time should be reduced to less than 10 s.

3.2.5 Summary and Status

Fifteen samples were prepared in three different matrices (five each for tap water, creek water, and soil/red clay). One blank was prepared, and four samples of each matrix were spiked with a target protein/organism. The target proteins/organisms used were melittin (100 and 1 nM final concentration), cholera toxin (1 µM final concentration), and bacteriophage MS2. A duplicate set of samples was prepared and was frozen at –70ºC for analysis later by the CBNP Block II CBMS instrument. Of the twelve samples analyzed by the advanced ion trap system, nine were correctly identified in their various matrices. All of the three missed samples were false negatives; no false positive results were obtained from this study. Samples could be confirmed as a positive via one of three methods: sequence tag identification (melittin), library matching (cholera toxin), and a newly developed computer interpretation algorithm. The cumulative results of the study are shown in Table 3.4.

The most difficult matrix encountered in this study was the creek water matrix. All three false negative samples were obtained for toxins/viruses spiked into this matrix. In the case of the 1-nM melittin sample, the signal-to-noise ratio for the mass isolation step of the precursor ion was not sufficient to produce reliable MS/MS data even though the sample was preconcentrated by using c_{18} material. For the two samples that were dialyzed (cholera toxin and bacteriophage MS2), no stable signal could be obtained, indicating the possibility of a strong matrix effect suppressing the electrospray signal. Even when an additional spike of cholera toxin was placed in the creek water sample after dialysis, no signal could be detected, thereby suggesting that this ion suppression effect was matrix-driven and not the result of free proteases due to bacterial lysis. This study indicates that further characterization of various environmental matrices will be necessary to understand the required systems integration approach needed for successful analysis of environmental matrices.

Table 3.4. Summary of test results

Sample No.	Content	Identification	False negative	False positive
		Tap water		
1	Blank	–	–	–
2	Melittin 100 nM	Yes	No	No
3	Melittin 1 nM	Yes	No	No
4	Cholera toxin 1 µM	Yes	No	No
5	Bacteriophage MS2	Yes	No	No
		Creek water		
6	Blank	–	–	–
7	Melittin 100 nM	Yes	No	No
8	Melittin 1 nM	No	Yes	No
9	Cholera toxin 1 µM	No	Yes	No
10	Bacteriophage MS2	No	Yes	No
		Soil/red clay		
11	Blank	–	–	–
12	Melittin 100 nM	Yes	No	No
13	Melittin 1 nM	Yes[a]	No	No
14	Cholera toxin 1 µM	Yes	No	No
15	Bacteriophage MS2	Yes	No	No

[a]Identified at the minimum signal-to-noise ratio.

Overall, we are very optimistic about the future of this electrospray/ITMS approach to biological weapons detection. Current laboratory equipment and methods are not yet optimized for sensitivity or speed of analysis. Work to date has revealed no impediments to successful integration of this technology for deployment on the Block II CBMS platform (although methods development is continuing). Hardware for retrofitting this technology to the Block II CBMS platform could be developed in parallel with methods refinements and optimization.

REFERENCES

Barshick, S.A., D.A. Wolf, and A.A. Vass 1999. "Differentiation of Microorganisms Based on Pyrolysis-Ion Trap Mass Spectrometry Using Chemical Ionization." *Anal. Chem.,* 71, 633–41 (1999).

Basile, F., et al. 1998. "Direct Mass Spectrometric Analysis of in Situ Thermally Hydrolyzed and Methylated Lipids from Whole Bacterial Cells." *Anal. Chem.,* 70, 1555–62.

Cargile, B. J., S. A. McLuckey, and J. L. Stephenson, Jr. 2000. "Rapid Identification of Bacteriophage MS2 Coat Protein from E. Coli Lysates via Ion Trap Collisional Activation of Intact Protein Ions in Conjunction with Ion-Ion Reactions." *Anal. Chem.* 73, 1277–85.

Gieray, R. A., et al. 1997. "Real-Time Detection of Individual Airborne Bacteria." *J. Microbiol. Methods* 29, 191.

Hart, K. J., et al. 2000. "Design, Development, and Performance of a Fieldable Chemical and Biological Agent Detector." *Field Analytical Chemistry and Technology* 4 (22-3), 93–110.

Lammert, S.A., et al. 2001. "Optimization and performance of a Toroidal Ion Trap Mass Spectrometer." *Int. Journal Mass Spectrom.* 212 (1–3), 25–40.

Parker, E. P., et al. 2000. "Detection and Classification of Individual Airborne Microparticles Using Laser Ablation Mass Spectroscopy and Multivariate Analysis." *Field Analytical Chemistry and Technology*, 4, 31.

Stephenson, Jr., J., B. J. Cargile, and S. A. McLuckey 1999. "Ion Trap Collisional Activation of Disulfide Linkage Intact and Reduced Multiply Protonated Polypeptides." *Rapid Comm. Mass Spectrom.* 13, 2040–48.

Yang, M., et al. 1996. "Real-Time Chemical Analysis of Aerosol Particles Using an Ion Trap Mass Spectrometer." *Rapid Comm. in Mass Spectrom.* 10, 347.